Carbonaceous Nanoparticle Molecular Inception from Radical Addition and van der Waals Coagulation of Polycyclic Aromatic Hydrocarbon-Based Systems. A Theoretical Study.

UNIVERSITÀ DEGLI STUDI DI TORINO

CARBONACEOUS NANOPARTICLE MOLECULAR INCEPTION FROM RADICAL ADDITION AND VAN DER WAALS COAGULATION OF POLYCYCLIC AROMATIC HYDROCARBON–BASED SYSTEMS. A THEORETICAL STUDY.

Anna Giordana, Andrea Maranzana, and Glauco Tonachini*

Dipartimento di Chimica Generale e Chimica Organica, Università di Torino,
Corso Massimo D'Azeglio 48, I-10125 Torino, Italy

Abstract. Carbon nanoparticles, generated during combustion at relatively low [O_2] or under pyro-lysis conditions, can be seen both as soot precursors and as primary pollutants in themselves. Soot particle inception, with transition of relatively low-mass molecular systems from the gaseous phase to a solid nature through coagulation/condensation, is believed to take place via chemical reactions as well as van der Waals (vdW) interactions involving polycyclic aromatic hydrocarbons (PAHs) or derivatives. In this paper, radical addition between open and closed shell molecular PAH or PAH-like systems ($R^{\bullet} + P \rightarrow R{-}P^{\bullet}$) is examined by density functional theory, and different σ bond form-ations are compared with the stacking of the aromatic components ($R^{\bullet}$:P, previously discussed in *J. Phys. Chem. C* **2011**, 115, 1732–1739). Energetic and entropic effects are examined. At higher T, formation of aliphatic bridges (hence reticulation) appears to be of the utmost importance to link PAH-like moieties, with a preference for more extended arrangements (due to entropic effects). More packed structures, promoted by vdW interactions (an energetic effect), may be favored by lower T. Thus, when the gas in the flame cools down, reticulation could be followed by inter- or intra-molecular stacking. These distinct processes can take place within different T ranges, but are not mutually exclusive: in particular, σ bond formation helps subsequent stacking, since crystallites would be more easily produced at lower T by stacking of already bound elements. Therefore, the mechanistic picture offered by the calculations bears out a structural model for carbonaceous particle growth in which an initial more amorphous core is generated at higher T through successive radical attacks and σ bond formations, hence reticulation involving growing adducts of $R{-}P^{\bullet}$ type. The core can subsequently become enclosed in an external shell which grows at a lower-T regime and presents more ordered zones. It cannot be excluded that limited transitions from amorphous zones to more ordered zones could take place within internal regions of the particle, provided the local texture of these regions were sufficiently sparse to allow rotations in the $R{-}P^{\bullet}$ adducts from extended (anti) to packed (syn) arrangements.

Keywords: 1) carbon nanoparticles; 2) PAH radical addition; 3) PAH stacking;
4) density functional theory; 5) soot; 6) ultrafine particulate.

* e-mail: glauco.tonachini@unito.it - phone: ++39-011-6707648 - fax: ++39-011-2367648
group web site: http://www.thecream.unito.it/

suggested running title: C-nanoparticle inception

Introduction

Carbonaceous particulate is a significant contributor to the overall mass of atmospheric aerosol.[1,2] Its particles, of approximate spherical shape, are built by an irregular agglomerate structure of graphenic layers, which can be curved to different extents and present defects. More amorphous and more ordered zones coexist; the latter, called crystallites, appear as turbostratic stacks of PAH-like units. The globular particles (spherules) get further associated as clusters of different shapes.[3,4] Ultrafine molecular nanoparticles of size 1.5-4 nm have a likely role as precursors of carbonaceous particulate, and can also be emitted directly from combustion engines into the environment. They present a transition from the gaseous phase to a solid nature, and their generation modes are in part still to be clarified.[5,6] Ultrafine C-nanoparticles, identified under different conditions, in particular in flames, both under sooting or non-sooting conditions, can coexist with particles whose dimensions can exceed 10 nm, thus exhibiting an unimodal, bimodal or even trimodal nature.[7,8,9,10,11] Their multi-modal nature depends upon the *height above burner* parameter, z (hence also upon temper-ature).[12,13] Thus, a distinction can be drawn in some cases between primary particles (10-100 nm) and precursor nanoparticles (1-5 nm),[7a] in other cases among primary (20-50 nm), sub-primary (6-9 nm) and elementary (less than 5 nm)[14] particles, following di Stasio's classific-ation,[10,11] depending on the experimental conditions.

PAHs not only share the same nature and origin of soot platelets[15,16,17,18,19,20,21] but can also be found associated with soot.[22,23] They are often considered as its precursors, but other opinions have been put forth.[24] Homann put forward[15] that the reactions leading to PAHs could also bring about the formation of more irregular structures, called "aromers" (i.e. *aro*matic oligo*mers*, seen as precursors of soot and fullerenes: see ref. 15, in particular § 7.3, 7.4, 8, and Fig. 22 therein), starting from association between PAHs and subsequent H_2 losses. These intermediate structures (which could grow as cages with a higher or lower H content, and get some curvature) could be at the origin of either or both fullerenes and soot,[25] depending on the relative abundance of small growth components, as HCCH, and on temperature.

The generation modes of soot precursor nanoparticles, which is the subject of the present study, is a complex problem which stirs continuous interest in a vaste community.[26] It has been confronted by different experimental techniques,[10,11,26ab,27,28,29] and has also been the subject of some theoretical/computational investigations carried out at different scales and by different methods.[26cd,30,31,32,33,34,35,36,37,38,39] Useful accounts of the experimental evidences collected from the sixties up to now, concerning the generation and structural features of carbonaceous particles, can be found in

recent papers.[25,26ae, 29] These can be flanked by the interesting discussion on theoretical results that can be found in Frenklach's 2002,[40] Xi and Zhong's 2006,[41] Dobbins' 2007,[42] and Wang's 2011[43] review papers. Since some of the opinions based on experimental and theoretical results will be discussed in connection with our findings in the final part of the paper, we will now introduce some of them only briefly.

The structural details of the soot spheroidal particle bear an evident relation with the overall growth process phases. These are initially PAH combustive synthesis[40a] (notable, among the proposed mechanisms, Bittner and Howard's[44] and Frenklach's HACA[45]), as well as graphene edge growth.[38,46] Then, PAH stacking via van der Waals interactions [26c,36,37] (vdW for short in the following) and radical reactions[29,39] between smaller hydrocarbon constituents (Howard's "reactive coagulation")[47] can follow, in a sequence apt to build larger systems and give rise to carbonaceous particle inception. This last phase has been in fact taken into account in several papers in relation with the other aspects.[14,26,39,48,49,50,51,52,53] As regards the latter phases, D'Anna, for instance, came recently to the conclusion that (i) stacked PAH structures are favored by low T and low radical concentrations, but (ii) aromatic-aliphatic linked structures are formed when the chemical-growth mechanism is enhanced at higher temperatures and radical concentrations.[29] Then, Chung and Violi reported very recently[35] the interesting results of a Molecular Dynamics study, that can be summarized as follows. In the T range 1000-1500 K the physical formation of small PAH clusters is found, but they do not appear to be stable enough to allow a further growth and act as soot nuclei. Aromatics with an aliphatic chain have a faster nucleation rate than peri-condensed aromatics and aromatic molecules linked by aliphatic chains of similar mass. Thus chains could act as a sink to accommodate the collisional energy, facilitating the physical growth of clusters. However, physical nucleation is viable in the temperature range up to 750 K, but for temperatures higher than 1000 K a chemical mechanism (bonding between molecules) needs to be invoked. Coming now to the globular particle organization, earlier hypotheses, based on experimental findings, were reported in a 1982 paper by J. B. Donnet,[54] who proposed a particle structure where a more amorphous core was surrounded by a more ordered shell. Later on, as experimental techniques evolved, new results allowed to elaborate on further features.[10,11,26,27] Donnet's view was subsequently supported by Frenklach and Wang's computations,[45] and recently corroborated by Grotheer and coworkers, on the basis of experimental results.[26b,28] In particular, they used photoionization mass spectrometry to distinguish between two types of soot precursors, namely PAH stacks and PAH clusters held together by aliphatic bonds. Both possibilities had already been considered, as said, by different researchers. For instance, Schuetz and Frenklach,[26c,37] as well as Herdman and Miller,[36] put the accent, on the basis of computations, on the likelihood of PAH stacks able to survive at flame temperatures. On the

other hand, D'Alessio and coworkers indicated, on the basis of experimental results, that formation of high molecular mass PAH associations occurs through the polymerization of small PAHs.[49b]

We have recently studied by quantum mechanical methods the growth of an aromatic system adsorbed on a model soot platelet,[55] and the feasibility of association of PAHs via vdW interaction.[56,57] In the latter study it was concluded that, at high temperature, pure vdW stacking can hardly be a major factor in triggering soot nano-particle inception. In fact, though energetic effects would suggest that larger interacting systems will be better stabilized, entropy changes work in the opposite direction. In particular, the trends in Gibbs free energies are such that at higher temperatures the components of the largest systems are described to be prone to fly apart more than those of smaller systems, thus limiting the size of possibly forming crystallites. We now attempt, in the present study, to assess the importance, as a function of T, of a coagulation commencement by (A) radical addition and/or (B) vdW interaction. The temperature dependence of the processes A and B can affect the structure of the globular soot particles, whose growth proceeds at different T values. Therefore, we model by quantum mechanical methods the very initial nucleation steps, applied to PAH or PAH-like molecular systems, indicated as $R^{\bullet}$, a radical,[58] or P, a closed shell molecule (for PAH-like systems we intend either a PAH bearing an aliphatic chain substituent, or two PAH systems linked by aliphatic bridges or by a single σ bond). The initial molecular growth is thus described as taking place through radical addition of $R^{\bullet}$ to P, to produce a radical adduct $R{-}P^{\bullet}$, or association via vdW interaction between PAH-like sytems $R^{\bullet}$ and P of various sizes, to give complexes $R^{\bullet}$:P. Either process, or both, can be at the origin of coagulation (or condensation, depending on how is seen one of the two interacting systems).

Theoretical Method

All stationary points on the energy hypersurface, *i.e.* minima and first order saddle points, which correspond to transition structures (TS), are determined by gradient proced-ures[59] within the Density Functional Theory (DFT),[60] and making use of the M06-2X[61] functional. The M06-2X functional has been designed to allow the study of complexes of the vdW type, in which dispersion forces can play a significant or dominant role.[62] For this study in particular, it allows to define the interaction energies of graphenic, PAH-like, model systems. In recent years this functional has been tested,[63] for instance, on some aromatic systems, as peri-substituted biphenylene or corannulene and functionalized corannulene,[64] and different biomolecules.[65]

The standard sp basis set 3-21G[66] is here enriched with d functions on all carbons (with gaussian exponent = 1.0). The polarized split-valence shell basis set so defined is referred to as 3-21G(d) in this work, and used in all DFT calculations. The basis set flexibility is forcedly limited by the size of the systems studied: its dependability within the present study is discussed in the **Appendix**. The nature of the critical points is then checked by vibrational analysis, and the thermochemistry assessed (all vibrational frequencies are listed for all structures in the **Supporting Information**). On this basis, the zero point vibrational energies are estimated, and the relative energies corrected ($\Delta \boldsymbol{E}_{ZPE}$), then the relative enthalpies ($\Delta \boldsymbol{H}$) and Gibbs free energies ($\Delta \boldsymbol{G}$) are estimated for temperatures (reported in Kelvin degrees) ranging from room T up to those typical of combustion (300-2500 K).[12] All energetics is in kcal mol^{-1}.[67]

Whenever distinct moieties interact (as in R:P), or when two distinguishable parts of the same system show a vdW stacking due to multipolar and dispersion forces,[57] the Basis Set Superposition Error (BSSE) relevant to their interaction is accounted for by the counterpoise (CP) method.[68,69] When R• and P get linked (either by a simple σ bond or through an aliphatic chain previously formed as part of R•) the two interacting moieties are simply defined by the two reactants themselves (taken in their complex, TS, or adduct geometry).

All calculations are carried out by using the GAUSSIAN 09 system of programs.[70] The MOLDEN program is exploited to display the optimized structures.[71]

Results and discussion

The present study investigates the very first growth steps of PAH-like molecular systems, taking place either (A) through σ bond formation to chemically link them and/or (B) vdW association[57] to give a physical complex (stacking). These steps hint to the transition from composite but still rather low-molecular weight systems toward very small (solid state) particles. In case (A), soot nanoparticle inception can be modeled by the radical addition of an open shell PAH-like system R• to another closed shell PAH, P. Presumably, the radical attack can take place more easily by involving some border positions, where the spin density of R• and the electron density of P can present the largest values.[72] Upon addition, the adduct R–P• will bear some kind of σ bridge between the two carbons which become satur-ated. Stacking (B) of the R and P moieties might in principle precede σ bond formation but could also follow it (intermolecular or intramolecular stacking, respectively). The role of sheer intermolecular stacking to form a complex R•:P, which could be in itself a first step toward nucleation, was examined in a preceding paper.[56] If σ bond formation is instead the first step, the adduct geometry could tune, possibly through a simple conformational change, the interaction of the π systems initially belonging to the former R• and P moieties, and give way to some intramolecular stacking.

In a combustion environment, a large number of hydrogen atoms (and of other small reactive radicals, such as HO or O)[48ce,73] can be present, in such a way that it seems reason-able to imagine the odd-electron R• system generated either by H abstraction from a parent PAH[74] or by H addition to its π system. Alternatively, R• could also be chosen as an odd-π-electrons/odd-C-atoms PAH, having geometric and electronic structure similar to that obtained by H addition to a slightly larger molecule.[58] To explore the A and B processes, the following molecular model systems are chosen, based on the PAH or PAH-like systems of **Chart 1** (see also **Figures 1-4**). System 1 is defined by R• = $C_{16}H_9$• (1-pyrenyl) and P = $C_{42}H_{16}$ (tetrabenzo-[hi,jk,st,uv]ovalene). In R•, the unpaired electron is localized, as shown, in an approximately sp^2 in-plane carbon orbital. Once the attack of R• has been carried out onto P, a σ bond between sp^2 and sp^3 carbons has formed, to give a possible precursor of a biphenyl-like structure, upon subsequent H• loss from the latter. This kind of bonding has been discussed by Richter et al.[75] and by D'Anna and coworkers.[6,76,77] System 2 is defined by R• = $C_{16}H_{11}$• (1-*H*-pyrenyl) and P as above. In this case, the unpaired electron is delocalized on the π orbital system (only one resonance structure shown in **Chart 1**). Direct addition of the two molecules produces in these two systems stable situations where R and P get linked by a simple σ bond. Yet, in particular for system 2, the arrangement seems rather stiff, since the σ bond is anchored to deformed regions of the PAH-like parts, though they can rotate around it.

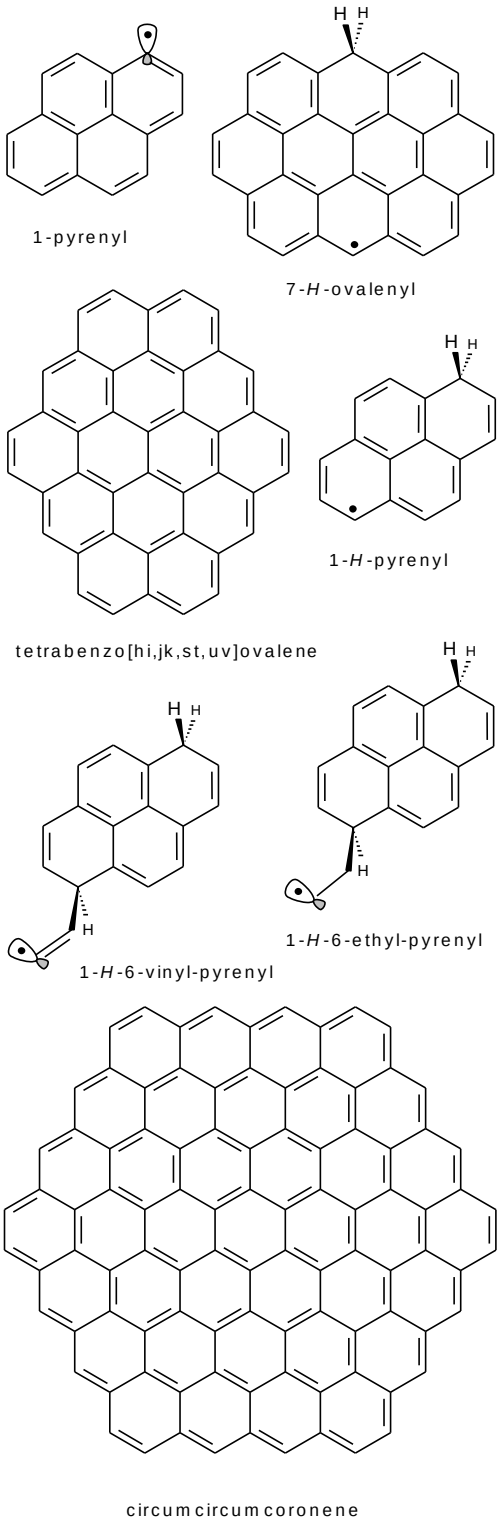

CHART 1. The molecular systems chosen to model nucleation.

Then, to explore the effect of size increase when the adduct formation is expected to present this rather rigid situation, system 3 is studied. It is similar to system 2, but with R• = $C_{32}H_{15}$• (7-*H*-ovalenyl) and P = $C_{96}H_{24}$ (circumcircumcoronene). This is followed by system 4, where we consider the preliminary formation of a radical aliphatic tail, by first

adding R′• (= 1-*H*-pyrenyl) to ethyne.[78] As in system 1, the unpaired electron is localized: here in an approxim-ately sp^2 orbital of the terminal vinyl carbon. Upon subsequent addition of the resulting R• = R′–CH=CH• radical to P, a rather bendable vinyl bridge forms. Similarly, by studying the addition of the same R′• to ethene,[78] a $-CH_2-CH_2-$ spacer is obtained to connect R and P (system 5). The choice of systems 1-5 has been one among many possible, hopefully a fairly realistic one. The largest dimensions of the heaviest molecular model ($C_{96}H_{24}$) are approxim-ately 1.9 nm. The corresponding R–P• or R•:P systems, which involve up to 128 C atoms, arrive at ca. 2.4 nm. The dimensions depend of course on the geometry, more crowded or more uncongested.

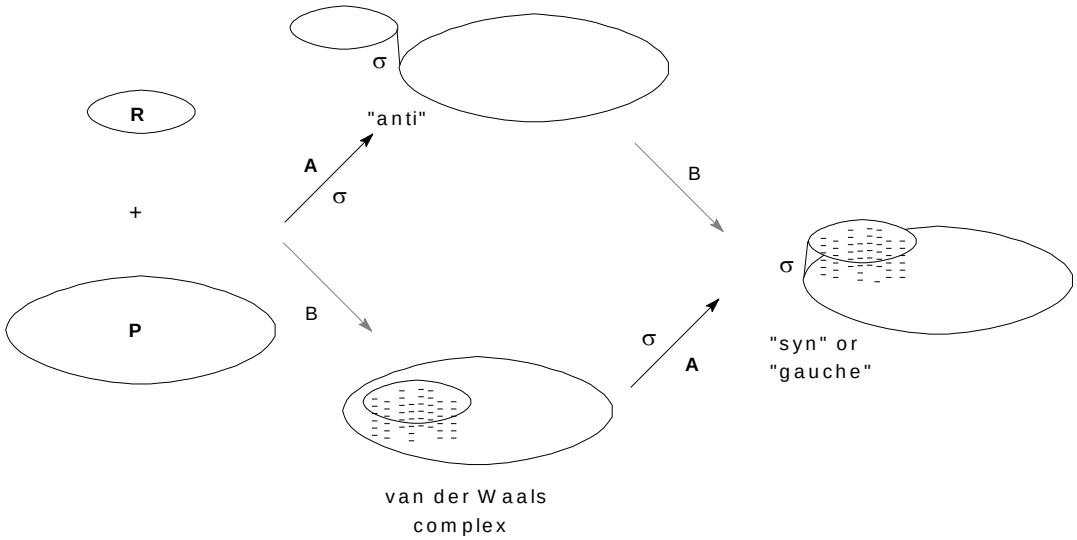

SCHEME 1. Two PAH systems, R• and P, interact first either (A) through formation of a σ bond, or (B) to form a vdW complex (left). Then, vdW interactions can induce a rotation around the newly formed bridge (top right, B) toward a more packed, approximately "gauche" or even "syn", arrangement (see Chart 2 for the use of these terms). Alternatively, (bottom right, A) a σ bond forms. Here a segment labeled **σ** symbolically indicates a simple σ bond connection or the presence of an aliphatic bridge.

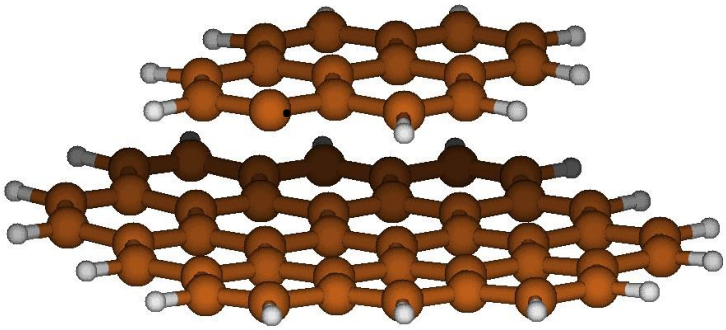

a

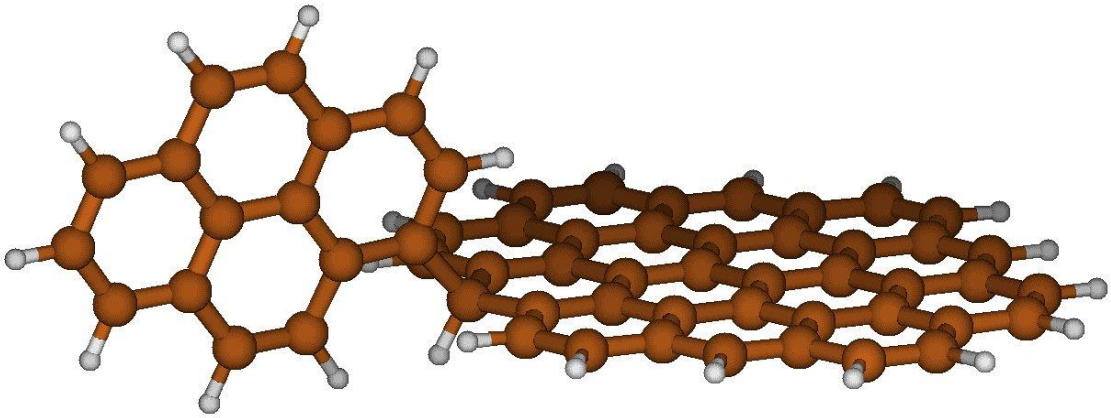

b

FIGURE 1. **System 1**. (a) vdW complex between $R^{\bullet}$ ($C_{16}H_9^{\bullet}$, where a dot indicates the radical site) and P ($C_{42}H_{16}$); it is also representative of the parallel arrangement found for the other systems. In $R^{\bullet}$, the unpaired electron is localized in an approximately sp^2 in-plane carbon orbital (here on top left, pointing toward the observer). (b) Adduct formed upon radical addition of $R^{\bullet}$ to P (the unpaired electron is now delocalized on the π system of the latter).

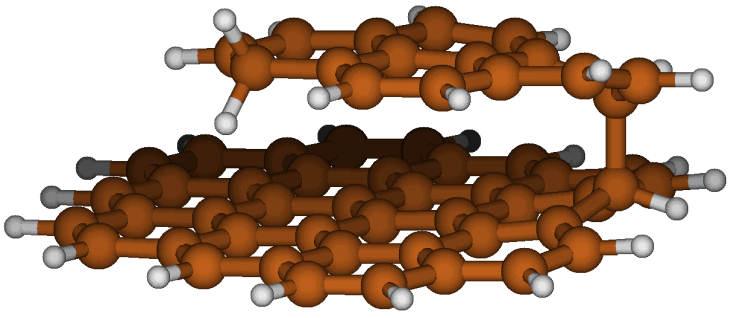

FIGURE 2. **System 2**. The radical attack of $R^{\bullet}$ ($C_{16}H_{11}^{\bullet}$, whose unpaired electron is delocalized on the π orbital system) onto P ($C_{42}H_{16}$) brings about the formation of a σ bridge. The unpaired electron is now delocalized on the π system of the latter. The approximately syn orientation of the adduct along the σ bond that connects R and P (see Chart 2) implies a good overlap of the two opposed π systems, in correspondence of which vdW forces operate an evident stacking. Rotation along the σ bond R–P connects it with an approximately gauche arrangement (not shown), where the overlap is less complete. The larger system 3 ($R^{\bullet} = C_{32}H_{15}^{\bullet}$, $P = C_{96}H_{24}$) presents a similar situation.

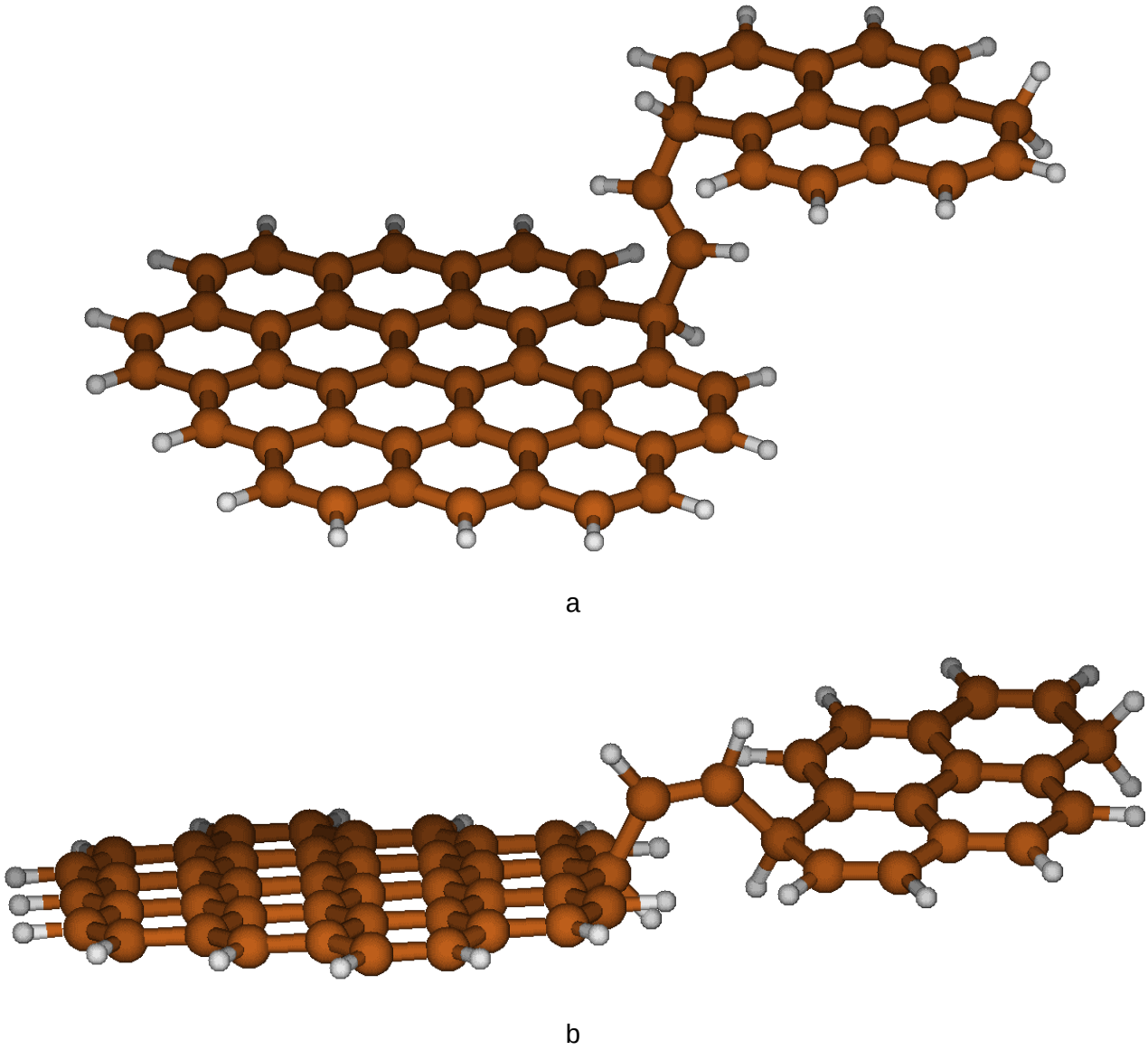

a

b

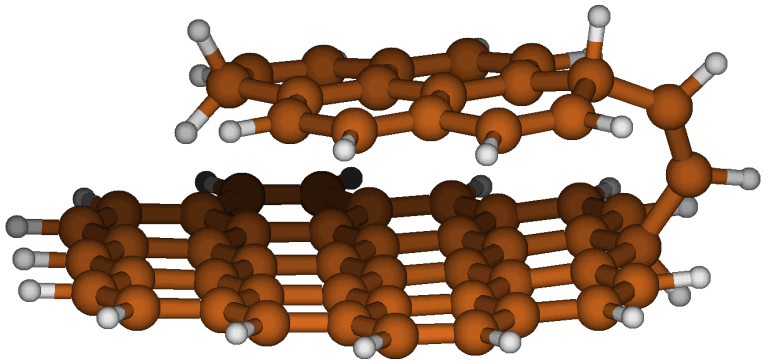

c

FIGURE 3. **System 4**. (a) Trans adduct, in an approximately anti orientation, as defined in Chart 2, formed upon addition of R'–CH=CH$^{\bullet}$ to P (where R' = $C_{16}H_{11}^{\bullet}$ and P = $C_{42}H_{16}$ (denoted as anti trans). (b) Cis adduct, again with an anti orientation (anti cis). (c) A syn cis form in which vdW interactions operate a stacking of the PAH-like parts. Rotations along the single carbon-carbon bonds of the aliphatic C–CH=CH–C bridge can connect structures 3b and 3c within the cis arrangement. A packed syn form of trans similar to 3c cannot instead be determined, since the PAH-like parts are forced to diverge by the bridge geometry. In all cases the unpaired electron is again delocalized on the former P's π system.

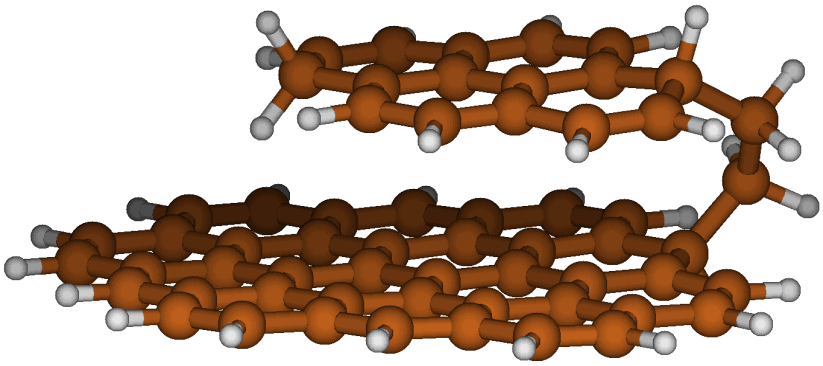

FIGURE 4. **System 5**. The adduct formed upon addition of R'–CH_2–$CH_2^{\bullet}$ to P (where R' = $C_{16}H_{11}^{\bullet}$ and P = $C_{42}H_{16}$), where vdW interactions induce again a stacking of the PAH-like parts and a syn arrangement.

In this section, we will address the following points.

(1) ***Stacking vs σ bonding* at the onset of nanoparticle formation.** Two PAH systems, R$^{\bullet}$ and P, could first interact either through process A, possibly followed by process B, or vice versa (**Scheme 1**). Once the new σ bond (possibly involving an aliphatic bridge) is formed, torsions along it can occur, and conformational preferences can emerge.[79] Therefore, we aim to assess if a packed arrangement of the two unsaturated sub-systems can be the most stable. This means, in

systems 2-5, a preference for an approximately syn conformation of R and P around the new σ bond. The use of the labels anti, syn, and gauche -made at liberty in this context- is illustrated in **Chart 2** and **Figures 2-4**. In the packed arrangements, vdW forces are of course most effective. As an alternative, a less crowded arrangement might be preferred, and it would correspond to an approximately anti conformation in which the vdW interact-ions operate in the least effective way. Approximately gauche arrangements are conceivable as intermediate possibilities. In the first case, one could speak of "steric attraction",[80] due to vdW interactions, and stacking preceded (or even promoted) by bonding would occur. On the other hand, an initial stacking of R and P does not exclude in principle the subsequent formation of a σ bond (**Scheme 1**, lower pathway).

(2) ***Temperature dependence of stacking and σ bond formation.*** We aim also to appraise how the initial nanoparticle nucleation process can be affected by temperature, as regards its mode (point 1 above) and viability. A dependence on T can be foreseen for both A and B processes. Therefore, we will assess the changes in Gibbs free energy $\Delta G(T)$ as stacking or σ bond formation take place.

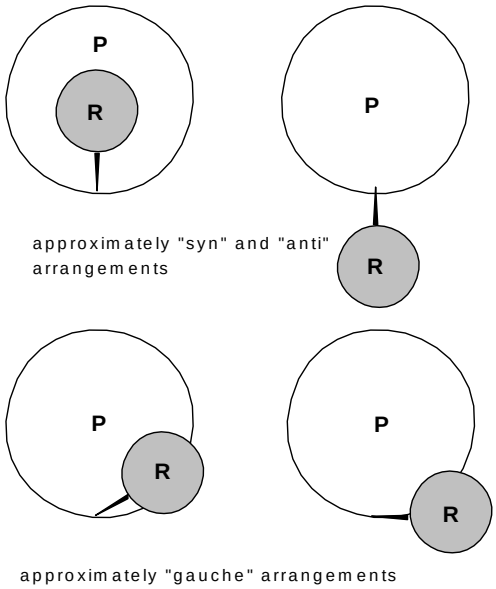

CHART 2. How the labels "syn", "anti", and "gauche" are loosely used in this context for the R–P adducts. A wedge indicates the new σ bond or an aliphatic bridge. In some case, not all the conceivable arrangements are found (see note 79).

The energetics relevant to the structures optimized for systems 1-5 is reported in **Table 1**. **Figures 1-4** display some of the structures. As regards point 1, we will first single out the counterpoise- and ZPE-

corrected energy differences and briefly discuss their values in connection with electronic and structural features of the initial vdW complexes and radical addition products for systems 1-5. Then, making reference to point 2, we will offer an interpretation of the ΔG(T) changes for the vdW complexes, transition structures, and adducts, in terms of balance of energy and entropy effects. The ΔG variations as a function of T are displayed in **Figure 5**. Finally, we will set forth an equilibrium hypothesis and try to bear it out for some temperature range: we will consequently turn our attention to the thermodynamic K values, which reflect the stabilities of complexes and adducts, as estimated from the same computed free energy differences. The thermodynamic stabilities of complexes and adducts are represented as pK(T) values in **Figure 6**. On that basis, we will put forward a hypothesis as regards soot nuclei growth.

Stacking vs σ bond formation: energy changes.

Figure 1a exemplifies a complex, shown only for system 1 (those for the other systems are similar). The parallel arrangement of the two moieties reflects vdW interactions, which in relatively large systems favor it with respect to a perpendicular layout, in which one molecule points with some C–H bonds towards the π system of the other.[55,56] The ΔE_{ZPE} values with respect to the reactants will now be examined (**Table 1**). For the complexes of systems 1, 2, 4 and 5 we start from the not unexpectedly rather close values of ca. –16, -14, -12 and -11 kcal mol^{-1}, respectively. These complexes are structurally rather close, though some moderate increase in steric hindrance in going from the former to the latter can be presumed (system 2 has one H more on the border with respect to system 1, then system 4 and 5 have aliphatic groups). The complex of system 3 is located instead at -26 kcal mol^{-1}, reflecting the size increase and the consequently increased importance of vdW interactions. In 3, steric encumbrance, as can be generated by one H atom, can be supposed to be similar to that found in 2.

Coming to the adducts, for system 1 we find it at -40 kcal mol^{-1} (σ bond formation), comparable to those of system 4, where the trans arrangement is at -38 kcal mol^{-1}, quite close in turn to the anti cis, also at -38 (both have undergone only σ bond formation). In the more crowded syn cis arrangement, in addition to σ bond formation, vdW interactions can be set up profitably, as far as energy is concerned, and the adduct is somewhat more stable, at ca.
-44 kcal mol^{-1}. All these addition products benefit from noticeable extra stabilization. Actually, systems 1, 4, and (somewhat less so) 5 share two common traits. (i) They can accommodate the new σ bond without suffering deformations of the PAH-like parts. The deformation energies of the single R$^{\bullet}$ and P components in the adducts, together with the total R–P$^{\bullet}$ values, calculated with respect to reactants, are collected in **Table 1**, **Supporting Information**. (ii) Furthermore, the addition to the closed shell P molecule is carried out by a radical R$^{\bullet}$ which bears the unpaired electron in a localized (1 and 4: ~sp^2; 5: ~sp^3) C orbital: upon addition, a π-delocalized R–P$^{\bullet}$ adduct forms instead (sp$^{2\bullet} \rightarrow \pi^{\bullet}$ or sp$^{3\bullet} \rightarrow \pi^{\bullet}$). In the syn form of system 5, however, the energy drop for the molecular system is somewhat lower (syn: -29 kcal mol^{-1}) than that found in system 4 (syn cis: -44). This is mainly attributable to the deformation undergone by the two reacting species, mostly suffered by R$^{\bullet}$. In system 1, the energy gain implied by the vdW interactions present in the complex is thus bartered, when lost, with the more delocalized nature of the resulting radical. The

situation is much less favorable for the syn adducts of systems 2 and 3. They still retain the chief trait of the relevant complexes, the presence of vdW interactions, but are also, as anticipated, stiffly bound, in the sense that bond formation is allowed only by assuming a somewhat strained local geometry (deformation energies in **Table 1**, **Supporting Information**). In addition, they are π-delocalized systems before and after bond formation ($\pi^{\bullet} \rightarrow \pi^{\bullet}$). When compared to the sheer vdW stabilizing interaction present in the complexes, the situation is by and large worse. In fact, system 2 adducts have $\Delta \boldsymbol{E}_{ZPE}$ = +6 (syn), +12 (anti), and +14 kcal mol^{-1} (gauche), with a destabilization with respect to the relevant complex of 20, 26 and 28 kcal mol^{-1}, respectively. The adducts of the larger system 3 are at -9 (syn) or +5 (gauche) kcal mol^{-1}, lower than the preceding ones. But the destabilization with respect to the complex is also in this case sizable, 17 or 31 kcal mol^{-1}, respectively, values not far from those of system 2.

Stacking vs σ bond formation: free energy temperature dependence.

Initial complexes. As regards the vdW complex stability at various temperatures, we can begin by noting, for all systems, the expected trend of the $\Delta \boldsymbol{G}$ values toward a larger and significant endoergicity as temperature rises (**Figure 5a**). Systems 2, 4 and 5 have a very close behavior: structural changes, as the aliphatic chain in 4 and 5, bear little consequences on the stability of these complexes, and their lines result almost superimposed. As seen before, the larger system 3 is the most stable in terms of $\Delta \boldsymbol{E}_{ZPE}$, and, for lower T values, it is still so also in terms of $\Delta \boldsymbol{G}$. But its $\Delta \boldsymbol{G}$ line has a larger slope, in such a way that the complex of 3 becomes less stable at the highest temperatures. Notwithstanding the important energetic effect due to the greater influence of vdW interactions, as T rises, the difference in free energy differences between the systems dwindles away. By contrast, system 1, which starts grouped with 2, 4, and 5, departs from all others, since it exhibits a smaller slope. This feature is due to the -TΔS term in $\Delta \boldsymbol{G}$, which obviously favors the two separated molecules, more significantly at higher temperatures. It affects the slope of the various lines to a different degree, more so, and in an adverse way, for the larger, hence more constrained, system 3. In **Table 1** we can in fact read that the $\Delta \boldsymbol{S}$ contribution goes from –50 (system 1) to –55 or -56 cal mol^{-1} K^{-1} for systems 2, 4, and 5, whereas is -62 cal mol^{-1} K^{-1} for the larger system 3.

Table 1. Relative energies corrected by zero point vibrational energy ($\Delta \boldsymbol{E}_{ZPE}$), entropy differences ($\Delta \boldsymbol{S}$), and Gibbs free energy differences ($\Delta \boldsymbol{G}$).[a]

	$\Delta \boldsymbol{E}_{ZPE}$	$\Delta \boldsymbol{S}$[b]	$\Delta \boldsymbol{G}$

T /K :		300	300	900	1300	1700	2100	2500
SYSTEM 1								
complex R•:P	-15.6	*-49.8*	-0.5	27.9	45.8	63.2	80.2	96.9
addition TS	0.6	*-39.5*	12.8	35.7	50.4	64.9	79.2	93.3
adduct R–P•	-40.4	*-42.6*	-27.5	-2.9	12.7	27.8	42.5	56.9
SYSTEM 2								
complex R•:P	-14.3	*-56.2*	2.3	34.7	55.4	75.6	95.5	115.0
syn addition TS	7.1	*-58.3*	24.1	58.5	80.9	103.1	125.1	146.9
syn adduct R–P•	5.7	*-58.1*	22.5	56.5	78.7	99.7	120.7	141.4
anti addition TS	18.4	*-45.8*	32.1	59.1	76.6	94.0	111.1	128.1
anti adduct R–P•	12.3	*-46.5*	26.2	53.3	70.6	87.5	104.0	120.2
gauche addition TS	17.5	*-53.7*	33.1	64.9	85.4	105.8	125.9	145.8
gauche adduct R–P•	13.8	*-53.8*	29.5	60.6	80.5	100.0	119.1	137.9
SYSTEM 3								
complex R•:P	-26.3	*-62.2*	-8.0	27.9	50.9	73.3	95.4	117.2
syn addition TS	-5.2	*-69.0*	14.6	55.3	81.8	108.1	134.2	160.2
syn adduct R–P•	-9.0	*-67.8*	10.7	50.1	75.5	100.4	124.9	149.1
anti addition TS	8.7	*-48.6*	23.4	51.7	70.0	88.1	105.9	123.5
anti adduct R–P•	1.8	*-49.7*	16.7	45.6	63.9	81.8	99.3	116.5
gauche addition TS	9.5	*-52.5*	25.1	56.0	76.1	96.0	115.6	135.1
gauche adduct R–P•	4.6	*-53.6*	20.6	51.8	71.7	91.2	110.3	129.2
SYSTEM 4[c]								
complex R•:P	-12.4	*-55.0*	4.0	35.6	55.6	75.2	94.5	113.4
trans addition TS	1.9	*-42.4*	14.7	39.4	55.4	71.2	86.9	102.4
trans adduct R–P•	-38.1	*-45.0*	-24.8	1.7	18.8	35.5	51.8	67.8
syn-cis addition TS	-4.3	*-60.7*	13.2	48.8	72.0	94.9	117.7	140.3
syn-cis adduct R–P•	-44.5	*-62.1*	-26.8	9.9	33.6	56.9	79.8	102.3

anti-cis addition TS	2.4	*-39.7*	14.5	37.5	52.4	67.0	81.5	95.8
anti-cis adduct R–P•	-37.9	*-41.8*	-25.5	-0.9	14.8	30.0	45.0	59.6
anti → *syn cis* adducts[d]	-6.6	*-20.3*	-1.3	10.8	18.8	26.9	34.8	42.7
SYSTEM 5[e]								
complex R•:P	-10.5	*-55.7*	6.1	38.2	58.6	78.6	98.2	117.4
syn addition TS	4.0	*-60.6*	21.2	57.0	80.6	103.9	127.0	150.0
syn adduct R–P•	-28.9	*-64.1*	-10.8	27.6	52.7	77.4	101.7	125.8
gauche addition TS	3.5	*-56.9*	19.8	53.5	75.6	97.5	119.2	140.8
gauche adduct R–P•	-32.7	*-61.5*	-15.3	21.4	45.3	68.9	92.1	115.1

[a]With respect to reactants. Units: T in Kelvin degrees (K), $\Delta \boldsymbol{E}_{ZPE}$ and $\Delta \boldsymbol{G}$ in kcal mol^{-1}, $\Delta \boldsymbol{S}$ in cal mol^{-1} K^{-1}. Thermochemistry (ZPE contribution, $\Delta \boldsymbol{H}$, $\Delta \boldsymbol{S}$) computed in correspondence of the 3-21G(d) energies and optimized structures. [b]$\Delta \boldsymbol{S}$ is reported here only at T = 300 K: as regards its (moderate) variation in function of T, a full set of data is reported in the Supporting Information, Table 2. [c]R• from addition of the π radical PAH system R'• onto ethyne (system 4) to give R'–CH=CH•, where the unpaired electron is localized in an approximately sp^2 orbital of the terminal carbon atom. [d]Differences between the two minima (syn, packed – anti, extended). [e]R• from addition of the π radical PAH system R'• onto ethene (system 5) to give R'–CH_2–CH_2•, unpaired electron in a sp^3. An anti conformation could not be found.

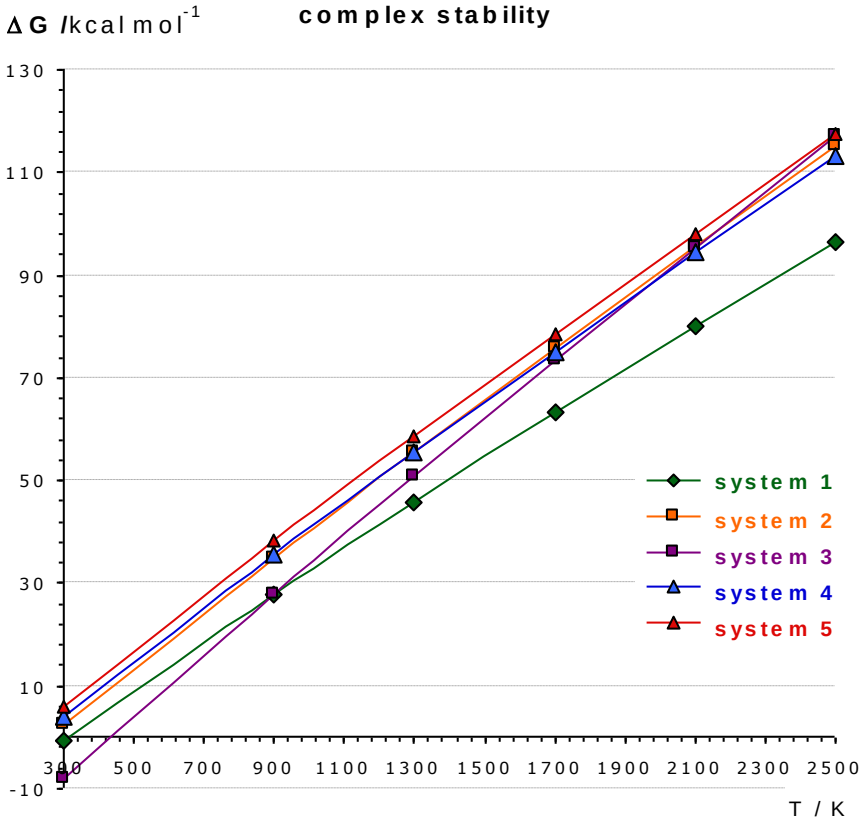

a

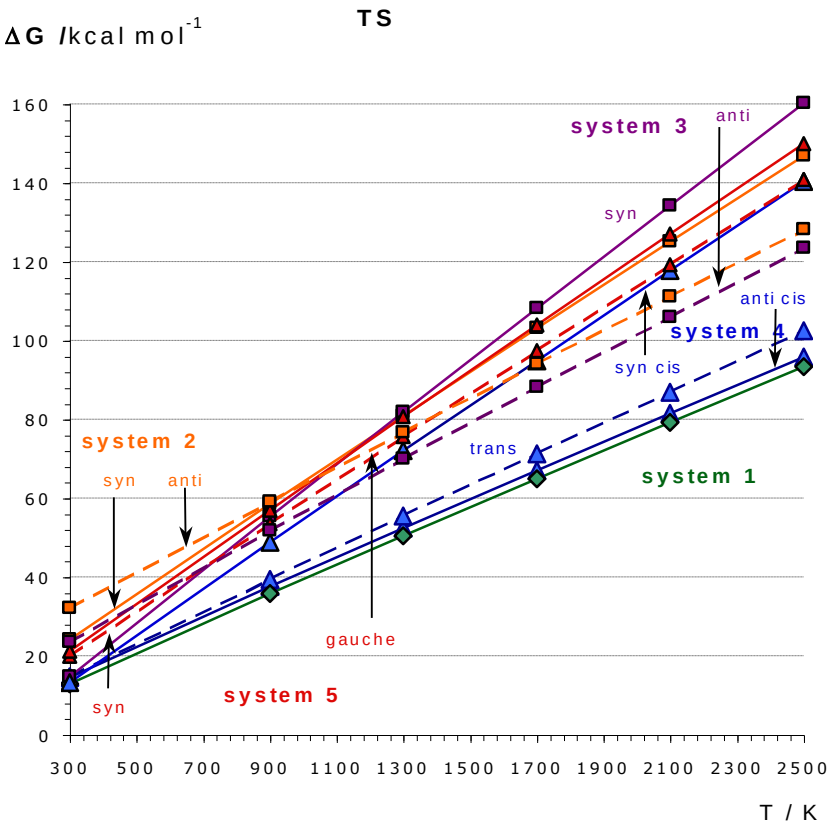
TS
ΔG /kcal mol-1
160
140
120
100
80
60
40
20
0
300
500
700
900
1100
1300
1500
1700
1900
2100
2300
2500
T / K
system 3
anti
syn
anti cis
system 4
syn cis
system 2
syn
anti
trans
system 1
gauche
syn
system 5

b

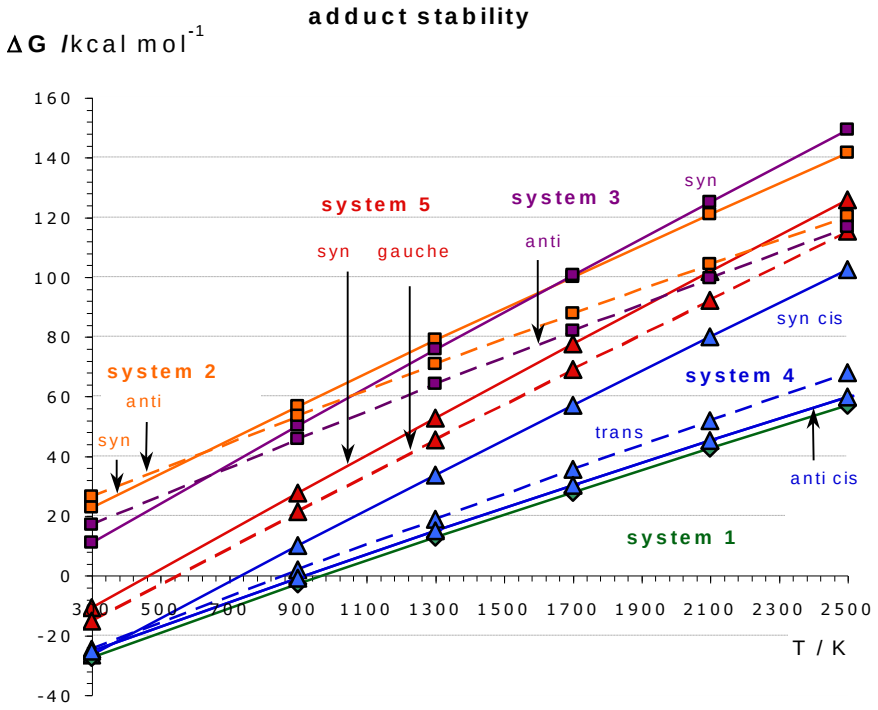

c

FIGURE 5. ΔG for the four models with respect to reactants for (a) van der Waals complexes; (b) transition structures for radical addition; (c) adducts. System 1: green, diamonds. System 2: orange, squares. System 3: purple, squares. System 4: blue, triangles. System 5: red, triangles. The less crowded arrangements correspond to dashed lines, the more packed to continuous lines.

The main point is however that, though the largest system is the stablest in a large T range, the complex stability in terms of steeply rising ***G***(T) differences with respect to the reactants seems to be in all cases very modest at combustion temperatures.

Transition structures and adducts. These will be discussed together, since the same features that begin to show up in a TS (**Figure 5b**) are fully present in the relevant addition product (**Figure 5c**). For all systems we find positive slopes of the ΔG lines. Systems 2, 3, and 4 present, within each system, a crossing upon T increase. All systems but system 1 (**Figure 1**) have more crowded structures, which we call syn following Chart 2. These packed arrangements "start" lower in most cases when ΔE_{ZPE}, or ΔG at 300 K, is considered as a reference. System 5 appears as an exception because the crossing is absent, and gauche is already lower in terms of ΔE_{ZPE}. The crossing appears because the ΔG line of each more extended

arrangement (anti for systems 2-4, but gauche for system 5) presents a less pronounced slope. For system 2 (see **Figure 2**) the syn-anti crossing occurs around 1000 K (TS) or 700 K (adduct), while for system 3 the crossing is at ca. 800 K (TS) or 700 K (adduct). At variance with this pattern, the diverging lines of system 4 may deceptively seem a different case. Actually the anti cis and syn cis lines just exhibit a much earlier convergence, around T=350 K. System 5 follows even more markedly this trend, and presents almost parallel lines.

Just in terms of $\Delta \boldsymbol{E}_{ZPE}$, the syn orientation in system 2 would be lower than the corresponding gauche or anti by 10 and 11 (TS) or 7 and 8 (adduct) kcal mol^{-1}. Similarly, in system 3 the anti and gauche TS are higher by 11 and 14 kcal mol^{-1}, respectively, and the adducts by 15, both. A larger vdW attraction for the syn determines the basic *energetic* trait upon which the $-T\Delta \boldsymbol{S}$ term then acts. Consistently, in the larger system 3, the difference between the syn and anti adducts is approximately twice that seen in system 2, with the same qualitative trends. On the other hand, the presence of vdW forces is not the sole factor in determining these energetic preferences. The structural features can entail other aspects, as the very deformations the systems have to undergo to allow for a more packed spatial arrangement. This aspect is illustrated by the two aliphatic-bridge linked systems: in system 4 the more crowded adduct is again almost 7 kcal mol^{-1} below the extended adduct, contrasted by system 5, where the gauche adduct is energetically more stable than the syn. In system 4 (anti trans arrangement, plus anti cis and syn cis arrangements, all shown in **Figure 3**), if transition structures are at lower energies ($\Delta \boldsymbol{E}_{ZPE}$) than those of system 2 by 11-15 kcal mol^{-1}, the adducts are drastically more stable. This energetic features can be traced back to two factors. (i) The greater flexibility introduced by the aliphatic bridge, which can allow a better arrangement of the PAH-like parts. (ii) The $sp^{2\bullet} \rightarrow \pi^{\bullet}$ change which accompanies σ bond formation. Similar factors operate for system 1, which does not suffer a sizable deformation, and shows in fact an adduct stability ($\Delta \boldsymbol{E}_{ZPE}$) close to those of system 4. See in all cases the deformation energies reported in **Table 1**, **Supporting Information**.

When the $-T\Delta \boldsymbol{S}$ term becomes important, the contrast with the purely energetic arguments becomes more and more visible. As temperature rises, the lines show different slopes: the more congested structures are expectedly more penalized by the entropic term with respect to the extended ones, and the most crowded visibly suffer from a more sizable constraint. This effect is traceable back to the contributions of a significant number of low-frequency vibrational modes (also reported in the **Supporting**

Information). To illustrate this point, here, **Table 1** reports, a $\Delta S^{\ddagger}$ or ΔS contribution (at T=300 K) of –58 cal mol^{-1} K^{-1} for both the TS and syn adduct of system 2. For the larger system 3, –69 to –68 cal mol^{-1} K^{-1} values are read instead when the arrangement is syn. In the gauche geometry, the $\Delta S^{\ddagger}$ or ΔS values are slightly lower as well as closer, –53 to -54 cal mol^{-1} K^{-1} for both systems. For the anti arrangement of systems 2 and 3, these figures are even lower, ca. –46 and –49 cal mol^{-1} K^{-1}, respectively. As regards the aliphatic-bridge linked systems 4 and 5, $\Delta S^{\ddagger}$ or ΔS values of ca. –61 to –64 cal mol^{-1} K^{-1} are computed for the more crowded transition and adduct structures. The less crowded structures determined here differ significantly one from the other, and, consistently, the $\Delta S^{\ddagger}$ values of ca. –40 cal mol^{-1} K^{-1} of system 4 (the fully extended anti cis) are contrasted by the –57 (TS) to –61 (adduct) cal mol^{-1} K^{-1} of the still crowded gauche form of system 5. System 1, uncrowded, presents a value of ca. –40 and –43 cal mol^{-1} K^{-1}, similar to the uncrowded structures of system 4.

Then, examining in more detail system 4, we see in **Figure 5** that, in terms of ΔG, benefits from a greater stability at all temperatures when compared with the preceding two. The syn cis adduct is still more stable only at the lowest temperatures, where vdW forces can still overcome the influence of the entropic term. In fact, a crossing occurs with the anti cis and anti trans adduct lines already at ca. 400 K, and then, as temperature rises, the less constrained arrangements get increasingly more stable. Similar features are observed for the barriers. Indeed, **Table 1** shows large variations between the entropy differences for the adducts of system 4: $\Delta S^{\ddagger}$ = –62 vs –42 (and –45) cal mol^{-1} K^{-1} for syn cis vs anti cis (and trans), in the order. Similarly for the TS data: $\Delta S^{\ddagger}$ =–61 vs -40 (and –42) cal mol^{-1} K^{-1}. Therefore, the behavior of the ΔG(T) lines of system 4 is similar to those of systems 2 and 3, the only difference is that they converge and cross at much lower temperatures. In particular, the slope of the anti cis and trans lines reflects the fact that the entropic term is less penalizing than in the other cases.

System 4 illustrates that the two processes of bond formation and stacking are not mutually exclusive. Though they could in principle take place in any order, as displayed in **Scheme 1**, the above results stress in particular that *bond formation may help stacking*. In fact, this trait can be inferred from the inspection of the "complex R$^{\bullet}$:P" and "anti → syn cis adducts" lines for system 4 in **Table 1**: on one hand, sheer stacking of two independent

moieties, as that involved in complex formation, presents a more advantageous *energy* change when compared with the stacking involved in the 'anti cis 3b to syn cis 3c' transformation ($\Delta \boldsymbol{E}_{ZPE}$ = -12.4 vs -6.6); on the other hand, the relevant $\Delta \boldsymbol{S}$ values are -55 and -20 cal mol^{-1} K^{-1}, respectively. The combination of these two expected features determines a less detrimental $\Delta \boldsymbol{G}$ for stacking at the various temperatures if a σ bond between the two PAH-like elements is already present. Similar considerations can be drawn for system 5, but to a lesser extent.

Finally, the stability of system 1, TS and adduct, is again very close to those of the anti trans and cis forms of system 4, and slightly larger. These structures (adducts in **Figure 1b** and **Figure 4, a** and **b**) share the same trait, an extended, uncongested arrangement, with little interaction of the two PAH moieties that moderates the penalization by the entropic term. Thus, no constraints such those dictated by vdW interactions are present, and also no incipient deformation of the PAH-like parts such as those induced by the stiff σ bond formation in 2 and 3 is seen.

Equilibrium constants. We have discussed, up to now, the free energy dependence on T, to underline the different roles of the energetic term (to which the vdW interaction contributes) and the entropic term, which works against π–π association. We could assume at this point that, at temperatures typical of a flame (see, for instance, Fig. 2 of ref. 76), an equilibrium situation is established for each value of the *height above burner* parameter, $\boldsymbol{z}$.[81,82] Accepting the equilibrium hypothesis, which is indeed a delicate point,[83] we could choose to emphasize the role of the complex and adduct stabilities compared to the two reacting moieties. Then, we can examine the behavior of the thermodynamic K(T), as estimated from the above discussed $\Delta \boldsymbol{G}$ data (the chosen standard state is 1 atm). While the linear T dependence of the entropic term has the direct and evident influence on $\Delta \boldsymbol{G}$(T) just discussed, the variations of the thermodynamic equilibrium constant come out, by contrast, damped at the highest temperatures. The relevant pK dependence on T is shown in **Figure 6a** (adducts) and **Figure 6b** (complexes). We see in **Figure 6a** that: (i) while some values increase with T, some other instead decrease; (ii) the dependence on T of them all decreases as T increases. These features can be traced back to the variation of the

enthalpic and entropic components, since the pK dependence on T is expressed as pK(T) = $-\log_{10}[\exp(-\Delta H/RT) \cdot \exp(\Delta S/R)]$.

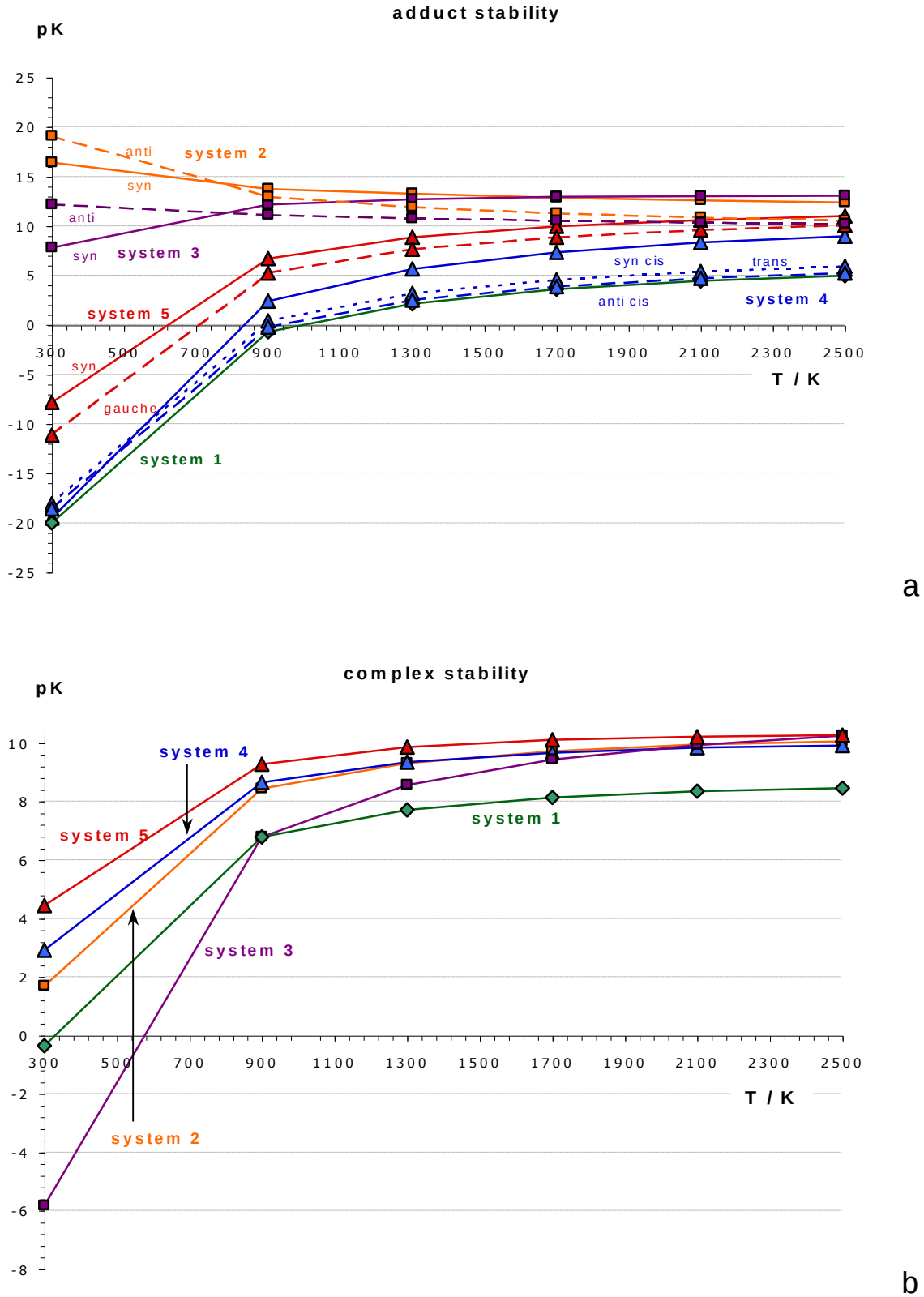

FIGURE 6. (a) Adduct and (b) complex stabilities with respect to reactants, for the four models, espressed as $pK(T) = -\log_{10}K(T)$. System 1: green, diamonds. System 2: orange,

squares. System 3: purple, squares. System 4: blue, triangles. System 5: red, triangles. (a) The more extended arrangements correspond to dashed lines, the more packed ones to continuous lines.

Incidentally, **Figure 7**, where we have reported, for sake of clarity, only the data for system 3, helps clarifying the origin of the different slopes and curvatures. Whilst both enthalpic and entropic terms exhibit only a limited and implicit T dependence, as $\Delta\boldsymbol{H}(T)$ and $\Delta\boldsymbol{S}(T)$ (dashed lines), the enthalpic contribution ($-\Delta\boldsymbol{H}/RT$, continuous lines) contains also a direct T dependence that combines with the implicit one; their combination determines the slope and curvature of the relevant lines (see **Table 3** in the **Supporting Information** for numerical values).

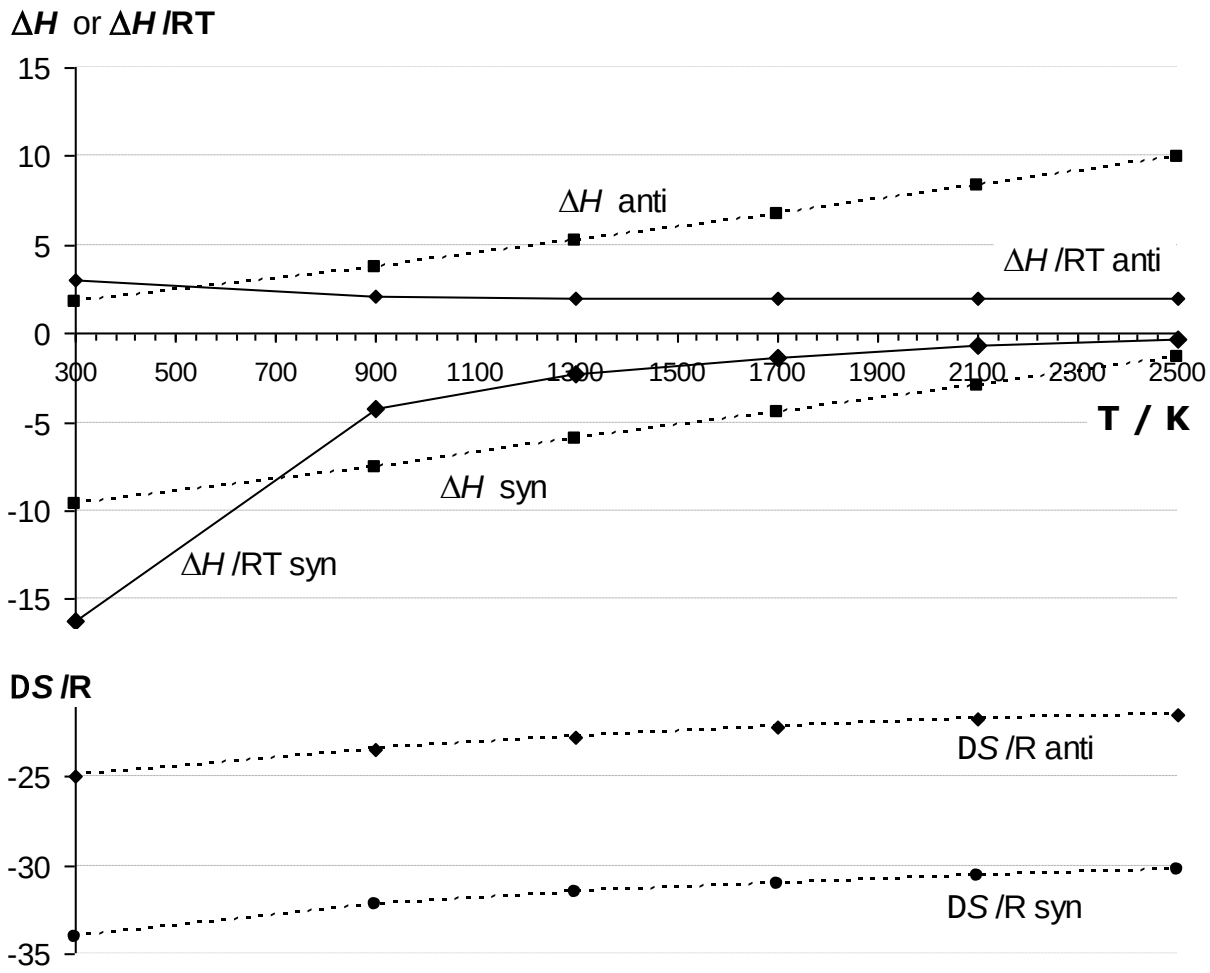

FIGURE 7. System 3: analysis of the behavior of $K(T) = \exp(-\Delta\boldsymbol{H}/RT)\cdot\exp(\Delta\boldsymbol{S}/R)$, in terms of the enthalpic and entropic components. $\Delta\boldsymbol{H}(T)$ (squares) and $\Delta\boldsymbol{S}(T)/R$ (circles) reported as dashed lines. $\Delta\boldsymbol{H}/RT$ (diamonds) reported as continuous lines. Units: $\Delta\boldsymbol{H}$ in kcal mol^{-1}, $\Delta\boldsymbol{S}$ in cal mol^{-1} K^{-1}.

Coming now back to the pK lines of **Figure 6a**, and keeping in mind a flame T profile as that just mentioned,[76] we can imagine them as "visited" by the evolving systems from right to left, if we suppose that carbonaceous nanoparticle growth can more easily proceed as T decreases. It can be observed that adducts of systems 1 and 4 are sharply favored (to a lesser extent also 5) with respect to 2 and 3 at all temperatures. The larger spread of pK values at low temperature can be thought of as reflecting the dominance of *energetic* factors. On the right, as we have seen, a higher temperature penalizes in particular all packed structures rather significantly. These are systems 2 and 3, the syn cis form in system 4, and system 5. A comparison can be drawn with the relevant complexes. This effect is reflected here by the higher pK values (**Figure 6b**). For instance, for systems 2 and 3 at T = 1100 K, pK ~ 14 and 12 (adducts), to be compared with pK ~ 9 and 8 (complexes), respectively. System 5 stays in between. System 3 is to a small extent favored because of its size and the consequent greater *energetic* role of vdW interactions. Then, at lower T and within each system, a syn form is *energetically* favored over an anti for the same reason (but it is not so for system 5). The leftmost part of **Figure 6a** indicates clearly these two trends. As regards the complexes (**Figure 6b**) the pK(T) lines reflect, at the lowest T, the effect of an increasing steric hindrance (hydrogens, aliphatic groups), and system 3 is the lowest as before. The obvious and dominant *energetic* factor is vdW stabilization, and is common to all structures. When the complex curves level off in correspondence of the highest temperatures, they converge with similar slopes towards a tight range of values, $8.1 \leq pK \leq 9.7$. An exception is 3, whose progress (slope and curvature) shows that it is more evidently penalized by the entropic term as T increases. By contrast, the pK curves of the adducts, though similarly damped, exhibit a larger variety of limiting values in correspondence of the highest temperatures, $3.6 \leq pK \leq 12.9$. Two distinct sets of values can be discerned, grouped toward these extremes.

Role of σ bond formation. The comparison between the adduct and complex curves allows, in fact, to appraise the particular *energetic* role of σ bond formation, and its weight in function of the characteristics of the addition step. If $R^{\bullet} + P \rightarrow R\text{–}P^{\bullet}$ entails a significant change in the radical nature, of the type $sp^{2\bullet} \rightarrow \pi^{\bullet}$ as in systems 1, 4 and 5, or a more modest change, of the type $\pi^{\bullet} \rightarrow \pi^{\bullet}$, as in the stiffly joint systems 2 and 3, we find striking differences that bear in the end some consequences as regards the picture of soot nanoparticle inception one can try to build. Thus, we have seen that, at combustion temperatures, formation of a σ bond, such as seen for systems 1, 4 and 5, seems to be the only viable step toward

association of PAH-like units. It appears consequently to be of paramount importance to start on coagulation, and feasible to some extent even at higher temperatures.

Sheer stacking has been indicated as a process likely to contribute to the onset of coagulation in recent and previous interesting works by Frenklach and coworkers.[26c,37] They carried out molecular dynamics simulations on rather small systems (e.g. pyrene and coronene dimers), setting T = 1600 K, and found appreciable dimer lifetimes. Also Herdman and Miller deemed that binding in PAH stacks is thermally likely at flame temperatures.[36] However, an opposing indication comes from other studies.[56,84] The present results suggest that, once very small nuclei are formed by σ bond linking of PAH-like units, when the gas in the flame cools down, this reticulation inception may be well accompanied by stacking. This possibility is suggested by the two curves of system 4 in **Figure 6a**, that exhibit, for the cis form, an anti $-$ syn crossing around T = 500 K. Bonds as that forming in system 1 do not obviously allow for any intramolecular piling. They do not exclude, on the other hand, the intervention of subsequent *inter*molecular stacking interactions, which are possible for all systems, and can consequently contribute to crystallite formation. Conversely, **Figure 6b** suggests that pure vdW $\pi-\pi$ association, as in the complexes, is unfavored, unless the interacting molecules or portions of soot lamellae were bearing quite large π systems. If we focus on crystallites and recall Frenklach's results,[26c] the necessity of definitely large PAH sizes to ensure some stability to a pure vdW complex seem in contrast with available experimental evidences on the limited size of such "graphitic domains".[85] It seems thus legitimate to suggest that the observed crystallites, which are *small*, are not held together by *pure* van der Waals interactions: when stackings are observed, these arrangements would have been made accessible to the local systems, on cooling down, by previous chemical bond formation.

Thus, reactive coagulation[47] can then open the way to further associations of separately formed molecular systems of the type $R-P^{\bullet}$. Reactive coagulation is actually invoked in several studies to account for the experimental results.[39,48] The present view, reticulation at higher T followed by stacking at lower T, is for instance in accord with the findings and conclusions of D'Anna.[29] He recently stated that stacked PAH structures are formed if the physical molecular growth mechanism, based on PAH dimerization, is favored by low T and low radical concentrations. Then that aromatic-aliphatic linked structures are formed when chemical-growth mechanism is enhanced, i.e. higher T and higher radical concentrations (p. 610 of ref. 29).

Our results are also in accord with the recent Molecular Dynamics study by Chung and Violi mentioned in the Introduction.[35] They found that the physical formation of small PAH clusters is possible within the T range 1000-1500 K. However these associations do not appear to be stable enough to act as soot nuclei. Aromatics with an aliphatic chain resulted to have a faster nucleation rate suggesting that chains could act as a sink to accommodate the collision energy and facilitate the physical growth of clusters. If, on one hand, physical nucleation resulted viable in the temperature range up to 750 K, they concluded that for temperatures higher than 1000 K a chemical mechanism (i.e. bonding between molecules) needs to be invoked.

Elementary particle structure. The present theoretical results suggest a reticulation commencement subsequently accompanied by stacking when the gas in the flame gets colder. This sequence implies in turn a particle structure with a more amorphous core enclosed in a locally more ordered external shell. This description corresponds to the early suggestion presented by Donnet,[54] backed then up by Frenklach and Wang's computations,[45] and recently put forward again by Grotheer and coworkers, on the basis of experimental results.[26c,28] It can be compared[86,87] (or contrasted[88]) with those described in other studies. In this respect, it is first worthwhile to consider in particular the interesting discussion in Frenklach's 2002 review paper. There, among other things, the role of different temperature regimes in favoring different growth processes is stressed.[40] Then, some prudence in drawing general conclusions on the structure of elementary particles is mandatory, since it is known that soot nanoparticles exhibit a structural dependence upon synthesis conditions, e.g. not only on temperature, but also on fuel, pressure, and flow rate. In this regard, also the overall origin (different diesel engines, spark discharges, furnaces, lamps) provides of course particulates characterized by structural differences. For instance, the experimental study by Müller, Su, Wild, and Schlögl, carried out by different techniques (HRTEM, EELS, XPS) on five different soots, stresses this point.[87] Also di Stasio and Braun compared soot from differ-ent sources to standard graphite by NEXAFS and introduced an *index of graphitization,* as the ratio I_π / I_σ (double and single bond peak intensities). I_π / I_σ has values 0.73 (diesel soot), 0.86 (ethene soot) 0.91 (carbon black) and 1.55 (graphite): see Fig. 1 and Table 2 in ref. 27. Also another study, by Vander Wal and Tomasek, can be mentioned to underline this aspect: they show that at lower T (1548 K) a more amorphous nanostructure is obtained, regardless of the other parameters; then, at

higher T (1956 K), other variables, namely fuel and flow rate, come into play, and nanostructures to a different degree curved or graphitic can be obtained.[89]

After these premises, we feel that our picture seems in agreement with the study just mentioned,[87] in which, for a model spark discharge soot and EuroIV soot, no specific core of particles like those typical of onion-like carbons could be identified, since the core of the particles was disordered. By contrast, for the more "graphitic" black smoke, furnace, and lamp soots the particles showed a core-shell morphology. Their nucleus was observed to form the highly disordered core, whose diameter was ca. 5 nm.

Our picture seems also in accord with the transmission electron microscopy (TEM) description of the "inner core particles"provided by Ishiguro, Takatori, and Akihama. They observed several fine particles of ca. 3 to 4 nm in diameter. The fine particle's nucleus had a diameter of ca. 1 nm, corresponding to several tens of atoms. The nucleus was covered by several carbon layers with a distorted, turbostratic structure. The outer shell was instead composed of microcrystallites, ca. 1 nm thick and 3.5 nm wide.[90]

Conversely, we see that the two-region model for an elementary particle, (inner amorphous core, outer shell containing crystallites),[54,27] also supported by our study, is at least partially contrasted first by Cain et al.,[88] and then by Wang's[43] proposals. Wang states that there is evidence that nascent soot from laminar premixed flames has a core–shell structure. Its aromatic core would be composed by small PAHs, as pyrene and ovalene, surrounded by an aliphatic shell. The latter would be responsible for the particle spreading into a flattened structure upon thermophoretic impact. Following Wang, the aromatic core is produced in the early stages of the flame where the gas temperature is high, while the aliphatic shell forms later, on the aromatic substrate, when the gas temperature becomes somewhat lower. The contrast is only partial, because our results agree with a core-shell structure and do not exclude the presence of aliphatics chains in the outermost zone of a globular particle. Yet, we find serious difficulties in imagining the formation of sheer vdW piles of aromatics to build up an inner core in an initial high-T phase, in particular if the intervention of limited-size PAHs is maintained.[43] As regards this point, we can imagine small aromatics only as parts of larger structures in which they are linked by aliphatic bridges or σ bonds. We could likewise envision that, upon thermophoretic impact (see Figure 18 in ref 43), an outer shell made in part of more ordered stacks could splatter as described by Wang. In fact, the aromatic components of a stack can very

easily slide in directions parallel to their molecular planes. It can be shown by a quantum mechanical computation, but is also witnessed in a very evident way by the "greasy" nature of graphite. Conversely, many σ bond formations could connect PAH-like components, since the process would be propagated by the odd-electron nature of the adducts so formed. They are representative of the persistent π radicals discussed by Wang in ref. 43, and could give way at higher temperatures to an inner nucleus characterized by reticulation and entropy-favored more pronounced disorder. This trait would entail an increase in the number of zones that contain sp^3 carbons, and the outcome could be a somewhat enhanced rigidity.[91] Within our picture, some transitions from amorphous zones to crystallites could however not be excluded from internal regions of the particle, formed at higher T. It could happen, provided their local texture were sufficiently sparse to allow structural changes as the anti – syn rotations in the R–P$^\bullet$ adducts discussed above.

To explain the observed effect of soot nanoparticle aggregates restructuring in flames, di Stasio proposed the abovementioned sliding of PAH-like planes.[92] Taking place at the points of contact between primary particles, it was at the origin of the shrinking of fractal aggregates as a transition from chain like to lumped aggregates. Numerical simulations of this effect were given by Dalis and Friedlander[93] and di Stasio and Iazzetta[94]. Then, the picture of the elementary particle structure apparently more consistent with our results (more amorphous core, locally more ordered outer shell) can be compared with di Stasio's interpretation of TEM images, offered in his 2001 paper.[11] There, the elementary particles, about 4 nm in size, observed in high concentrations, are described as composed by an inner core, whose size is 0.5-2 nm, opaque in the TEM images, and an external shell, with very regular size, transparent in the TEM micrographs. The nucleus was interpreted as a tangle of randomly oriented planes of graphitic nature, giving origin to destructive interference of the electron waves. The transparent shell was thought of as constituted of more crystallized carbon with lower electron density.

The random orientation of PAH-like planes in the particle core appears compatible with the higher-temperature reticulation suggested by our computations, since the core material would be consequently made up by the connection of randomly oriented PAH-like units through σ bonds or aliphatic bridges. Another interesting feature indicated by di Stasio[11] is that agglomeration is found for each of the three modes observed. In that paper it was demonstrated that primaries are in turns clusters of sub-primary

particles,[10] thus introducing the role of a hierarchic aggregation in soot formation processes. According to that scheme, agglomeration can start at any stage of nucleation. Furthermore, a fascinating aspect mentioned in his paper is the observed ability of the elementary particles to penetrate each other, only at an early stage of the nucleation phase and well before the complete formation of the elementary particles (ref. 11, p 114). This feature is suggested by his occasional observ-ation of inner cores of elementary particles which appear agglomerated in doublets.

This last trait appears to us, on one hand, inconsistent with a picture of particle nucleation onset based *only* on vdW-driven pilings of small aromatics. We reckon in fact that pure PAH piling-up*s* would be likely uneffective in establishing an inter-core agglomeration whatsoever, since forming new vdW interaction between PAH-like piles through interpenetration would destroy the original vdW interaction (much as in the reshuffling of a deck of playing cards, **Scheme 2a**).

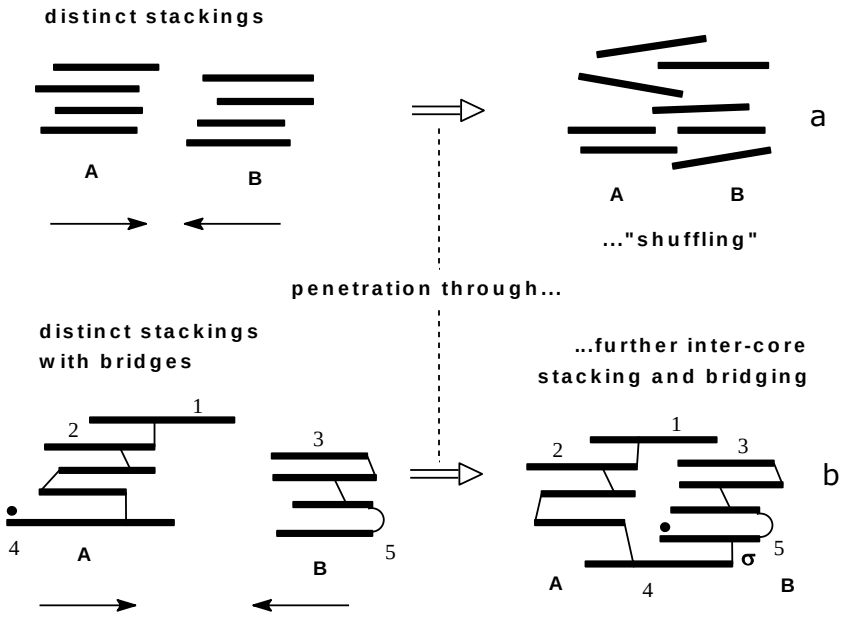

SCHEME 2. Simple representation of the compenetration (left to right) of inner elementary particle cores in an early phase of nucleation: interaction of two piles A and B, belonging to distinct particle cores, either (a) under the hypothesis that the nucleation onset relies on sheer vdW stacking of PAH units, or (b) surmising that some reticulation at higher T has to precede stacking at lower T.

On the other hand, if piles are imagined (**Scheme 2 b**) as held together not only by vdW interactions but also by aliphatic links of variable nature or σ bonds, inter-core interactions could be created (i) either

by simple rotations around the bridges, accompanied by new vdW interactions or (ii) by formation of inter-core aliphatic links or simple σ bonds. Both situations are naively illustrated in **Scheme 2** through sort of a side view. Sheet 1, formerly in vdW interaction with 2 (both belonging to core A), is shown in **b** as partially abandoning it, since it starts interacting with 3, belonging to core B, through vdW interactions. Notwith-standing this "partial partner change", it is still bound to its former partner by a aliphatic bridge or σ bond. Then, one unpaired electron, present on sheet 4, attacks 5 (new bond indicated by the label "σ"), which then will bear in turn one unpaired electron. Under hypothesis **b**, it seems more likely that the distinct but interacting cores can partially merge without losing their identity.

Conclusions

Energy and free energy. We considered the ΔE_{ZPE} and ΔG values, with respect to the reactants R• and P, for (1) the R–P• adducts and (2) their formation TS. We could assess that, whenever a tight, stiff connection entails some local deformation of the two linked unsaturated subsystems, a packed (syn) arrangement results in most cases more stable than a more extended one (anti) at the lowest temperatures. This translates for instance to the preference of the adducts of systems 2 and 3 for a syn conformation around the newly formed σ bond. In other words, "steric attraction", due to vdW interactions (an *energy* effect), can be discerned, though in general it becomes less pronouced and then desappears as T rises (due to an entropy effect, which is soon dominating; **Figure 5b**,**c**). The conflict between the two factors and the role of T are already evident when the sheer π complexes R•:P are considered (**Figure 5a**). A similar T effect is observed for system 4, in which a longer and more flexible aliphatic bridge (–CH=CH–) is present instead of a simple σ bond; but in this case we have found that the most congested arrangement, syn cis, is favored only at relatively low T, while the two less crowded arrangements, anti trans and anti cis, are preferred at most T values. System 5, which also bears an aliphatic $-CH_2-CH_2-$ bridge, shows a similar but smaller stability (**Figure 5b**,**c**). The comparison 4 vs. 5 offers an indication that vdW forces are not the only *energetic* factor in determining the best arrange-ment.

Therefore, intramolecular stacking (B) can or cannot accompany formation of a new σ bond (A), depending on the nature of the nature of the link between R• and P. Only system 1 cannot offer this choice, unless *inter*molecular stacking is also considered. A further feature indicated by the ΔG(T) plots is

that not only the introduction of a more flexible bridge, but also the absence of important deformations, are key factors that can help the adduct to better survive at higher temperatures. It can be seen in systems 1 and 4, when compared with 2 and 3; or, to a lesser extent and for a narrower T range, also in 5.

Thermodynamic equilibrium. Based on an equilibrium hypothesis,[82,83,95] relevant to $T \geq 1000$ K, we have examined the behavior of the thermodynamic K(T). While the linear T dependence of the entropic term has the said influence on $\Delta \boldsymbol{G}(T)$, the trends of the equilibrium constants (pK in **Figure 6**) are dictated by the $-\Delta \boldsymbol{H}/RT$ term, through a balance between the implicit $\Delta \boldsymbol{H}(T)$ and explicit (denominator) T dependencies. This effect is made more understandable by the inspection of **Figure 7**. As a consequence, the values of pK(T) come out visibly damped at the highest temperatures. Systems 1 and 4 (to a lesser extent system 5) are clearly favored at all temperatures, and the relevant lines provide the information that, also at the highest temperatures, a limited number of molecules can still give an adduct in these systems. Therefore, formation of an aliphatic bridge, or even of a simple σ bond appears to be of the utmost importance to get an association of two PAK-like moieties. This is true, provided a too stiff R–P connection with local deformation is avoided - as is avoided in system 1. Linking via σ bond can further propagate, since it is a process of radical nature. But when the gas in the flame cools down, this reticulation commencement might be accompanied by stacking. System 4, in particular, illustrates that the two processes of σ bond formation and stacking are not mutually exclusive, and *bond formation helps stacking*. This feature is indicated by the crossing that occurs at low temperatures between the cis adduct pK curves of the anti and syn structures. This supportive effect relies on the fact that the $\Delta \boldsymbol{S}$ is relevant in this case to the stacking of two already bound moieties, and consequently determines a less unfavorable $\Delta \boldsymbol{G}$ at the various temperatures.

Globular particle model. From the above results, which take into account the role of entropy effects, it can be suggested that crystallites are not held together by pure vdW interactions ($R^{\bullet} + P \rightarrow R{:}P^{\bullet}$), and that, when stackings are observed, these could have been facilitated by previous chemical bond formation ($R^{\bullet} + P \rightarrow R\text{–}P^{\bullet}$). Moreover, when aliphatic bridges, or also simple tight σ bonds, connect PAH-like components without significantly deforming them, the process can be propagated by the odd-electron nature of the $R\text{–}P^{\bullet}$ adducts so formed. In this case, the inner nucleus of a nascent nanoparticle, forming at higher T, could be characterized by reticulation more than by stacking. $R\text{–}P^{\bullet}$ adducts of any size could be

representative of the persistent π radicals discussed by Wang in ref. 43, together with simple PAH-like systems bearing an odd number of π electrons.[58] If reticulation at relatively higher T is accompanied by subsequent intramolecular or intermolecular stacking, when the gas in the flame gets colder, the picture resulting from the present study offers a description of a particle structure in which a more amorphous core containing differently oriented aromatic PAH-like zones is enclosed in a locally more ordered external shell. The present study does not exclude neither the presence of "σ-link mediated" stackings in the inner zone, nor the presence of aliphatic tails in the outer zone.

Appendix

A calculation run with the same DFT functional M06-2X, in conjunction with better basis sets could probably produce more accurate results, but the size of the systems investigated in this work does not allow to proceed beyond 3-21G(d).[66] To appraise how this restraint can affect the results discussed, two models are chosen. The small reacting systems are made either by (a) the phenyl radical + benzene ($C_6H_5^{\bullet}$ is a localized sp^2 radical) or (b) cyclohexadienyl radical + benzene (H-$C_6H_6^{\bullet}$ is a delocalized π radical) (**Scheme 3**). The two different radical additions form in both cases a π-delocalized radical adduct.

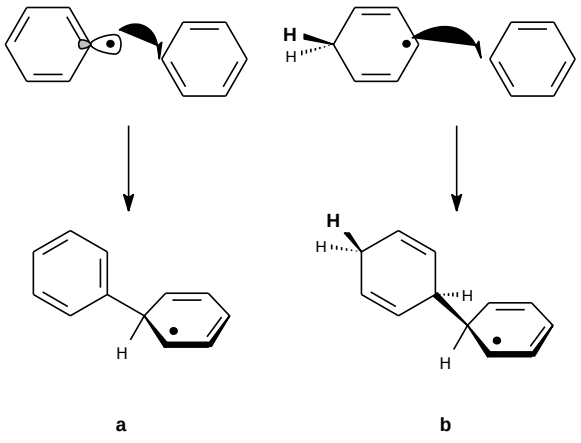

SCHEME 3. Model systems: addition to benzene of (a) the localized sp^2 radical $C_6H_5^{\bullet}$ and (b) the π-delocalized cyclohexadienyl radical.

The CP-corrected Gibbs free energy data (at T=298.15 K) obtainable at the 3-21G(d) level,[66] used throughout this paper, are compared with those provided by the more extended M06-2X/cc-pvTZ level.[96] Furthermore, the cc-pvTZ geometry optimizations can be followed by cc-pvQZ[97] single-point energy computations, to finally obtain M06-2X/CBS (complete basis set) estimates through an extrapolation

formula,[98] so providing a further reference. The values reported in **Table 2** indicate that the results obtained with the modest 3-21G(d) basis set can be sufficiently reliable.

Table 2. DFT/M06-2X relative free energies (kcal mol^{-1}).

ΔG at:	3-21G(d)	cc-pvTZ	cc-pvQZ	CBS
$C_6H_5^{\bullet} + C_6H_6$				
Addition TS	14.4	14.5	14.6	14.6
Adduct	-12.1	-11.7	-11.8	-11.9
$H\text{-}C_6H_6^{\bullet} + C_6H_6$				
Addition TS	32.3	32.4	32.3	32.3
Adduct	25.9	25.5	25.3	25.1

Acknowledgments

This work was conducted in the frame of EU ACCENT and ACCENT–PLUS (Atmospheric Composition Change, the European NeTwork of Excellence). An interesting discussion with dr. Stefano di Stasio from Aerosol and Nanostructures Lab at CNR-IM was most helpful to clarify some experimental aspects having a clear connection with our results.

Supporting Information for this article includes tables reporting deformation energies, ΔS(T), and ΔH(T) values, the geometries and energetics of all optimized structures, and all vibrational frequencies. This material is available free of charge via the Internet at http://pubs.acs.org.

References

[1] Cooke, W. F.; Wilson, J. J. N. *J. Geophys. Res.* **1996**, ***101***, 19395-19409.

[2] Liousse, C.; Penner, J. E.; Chuang, C.; Walton, J. J.; Eddleman, H.; Cachier, H. *J. Geophys. Res.* **1996**, *101*, 19411-19432.

[3] See for instance: Ivleva, N. P.; Messerer, A.; Yang, X.; Niessner, R.; Pöschl, U. *Environ. Sci. Technol*. **2007**, 41, 3702-3707, and: http://www.ws.chemie.tu-muenchen.de/groups/director projects0 /raman-soot/.

[4] Müller, J.-O.; Su, D. S.; Jentoft, R. E.; Wild, U.; Schlögl, R. *Environ. Sci. Technol*., **2006**, *40*, 1231-1236.

[5] D'Anna, A.; Commodo, M.; Minutolo, P. *Comb. Sci. Tech.* **2008**, *180*, 758-766.

[6] D'Anna, A.; Commodo, M.; Sirignano, M.; Minutolo, P.; Pagliara, R. *Proc. Comb. Inst.* **2009**, *32*, 793-801.

[7] See: fig 5 and 6 in (a) D'Anna, A. *Proc. Comb. Inst.* **2009**, *32*, 593–613; (b) fig 5 in Sgro, L.; Borghese, A.; Speranza, L.; Barone, A.; Minutolo, P.; Bruno, A.; D'Anna, A.; D'Alessio A. *Environ. Sci. Technol*. **2008**, *42*, 859–863.

[8] Öktem, B.; Tolocka, M. P.; Zhao, B.; Wang, H.; Johnston, M. V. *Comb. Flame* **2005**, *142*, 364–373.

[9] Abid, A. D.; Camacho, J.; Sheen, D. A.; Wang, H. *Comb. Flame* **2009**, *156*, 1862-1870.

[10] di Stasio, S.; Mitchell, J. B. A.; LeGarrec, J. L.; Bienner, L.; Wulff, M. *Carbon* **2006**, *44*, 1267-1279.

[11] di Stasio, S. *Carbon* **2001**, 39, 109-118.

[12] Temperature can span a significant range of values, depending on the type of experiment and its conditions. See for instance: (a) fig. 2 in Sirignano, M.; Kent, J.; D'Anna, A. *Comb. Flame.* **2010**, *157*, 1211-1219 (premixed C_2H_4/O_2 flame) and Fig. 2 in ref. 6 (soot forming flame SF22); (b) Alexiou, A.; Williams, A. *Comb. Flame.* **1996**, *104*, 51-65 (shock tube pyrolysis); (c) rif 13: Table 1.2, p 28 (flames with dioxygen or air as oxidizer).

[13] Glassmann, I.; Yetter, R. A. *Combustion* A.P. (Elsevier) 2008.

[14] D'Anna, A.; Commodo, M.; Minutolo, P. *Comb. Sci. Tech*. **2008**, *180*, 758–766.

[15] Homann, K.-H. *Angew. Chem. Int. Ed.* **1998**, *37*, 2434-2451.

[16] Finlayson-Pitts, B. J.; Pitts, J. N., Jr., *Chemistry of the Upper and Lower Atmosphere*; Academic Press, New York, 2000, ch. 10. See, in particular, Figures 10.2 and 10.3.

[17] Böhm, H.; Jander, H. *Phys. Chem. Chem. Phys.* **1999**, ***1***, 3775-3781.

[18] Ledesma, E. B.; Kalish, M. A.; Nelson, P. F.; Wornat, M. J.; Mackie, J. C. *Fuel* **2000**, 79, 1801-1814.

[19] Naydenova, I.; Vlasov, P. A.; Warnatz, J. *Proc. Eur. Comb. Meeting* **2005**.

[20] Jäger, C.; Huisken, F.; Mutschke, H.; Llamas-Jansa, I.; Henning, Th. *Astrophys. J.* **2009**, *696*, 706-712.

[21] Jäger, C.; Mutschke, H.; Huisken, F.; Krasnokutski, S.; Staicu, A.; Henning, Th.; Poppitz, W.; Voicu, I. *Astrophys. J. Suppl.* **2006**, *166*, 557-566.

[22] Pöschl, U.; Letzel, T.; Schauer, C.; Niessner, R. *J. Phys. Chem. A* **2001**, *105*, 4029-4041.

[23] Kamens, R. M.; Guo, J.; Guo, Z.; McDow, S. R. *Atmos. Environ*. **1990**, *24A*, 1161-1173.

[24] Siegmann, K.; Sattler, K.; Siegmann, H. C. *J. Electron Spectr.* **2002**, *126*, 191-202.

[25] Jander, H.; Wagner, H. Gg. *Comb. Explos. Schock Waves* **2006**, *42*, 696-701.

[26] See for instance: *Combustion Generated Fine Carbonaceous Particles*: Proceedings of the Anacapri International Workshop (Italy, 2007), Bockhorn, H.; D'Anna, A.; Sarofim, A. F.; Wang, H. editors; Doppiavoce, Napoli, Italy, 2009. In particular: (a) D'Anna, A. *Ch. 19*, pp 289-320. (b) Happold, J.; Grotheer, H.-H.; Aigner, M. *Ch. 18*, pp 277-287. (c) Wong, D.;Whitesides, R.; Schuetz, C. A.; Frenklach, M. *Ch. 16*, pp 247-287. (d) Miller, J. H.; Herdman, J. D. *Ch. 17*, pp 259-276.
(e) Dobbins, R. A. *Ch. 13*, pp 189-203.

[27] di Stasio, S.; Braun, A. *Energy & Fuels* **2006**, *20*, 187-194.

[28] Gonzalez Baquet, T.; Grotheer, H.-H.; Aigner, M. *Rapid Commun. Mass Spectrom.* **2007**, *21*, 4060–4064; in particular p 4064, and related references.

[29] D'Anna, A. *Proc. Comb. Inst.* **2009**, *32*, 593–613.

[30] Totton, T. S.; Chacrabarti, D.; Misquitta, A. J.; Sander, M.; Wales, D. J.; Kraft, M. *Comb. Flame* **2010**, *157*, 909-914.

[31] Violi, A.; Voth, G. A.; Sarofim, A. F. *Proc. Combust. Inst.* **2005**, *30*, 1343–1351.

[32] Chung, S. H.; Violi, A. *Carbon* **2007**, *45*, 2400–2410.

[33] Wang, D.; Violi, A. *J. Org. Chem.* **2006**, *71*, 8365-8371.

[34] Wang, D.; Violi, A. *J. Phys. Chem. A* **2006**, *110*, 4719-4725.

[35] Chung, S.-H.; Violi, A. *Proc. Combust. Inst.* **2011**, *33*, 693–700.

[36] Herdman, J. D.; Miller, J. H. *J. Phys. Chem. A* **2008**, *112*, 6249-6256.

[37] Schuetz, C. A.; Frenklach, M. *Proc. Comb. Inst.* **2002**, *29*, 2307–2314.

[38] Whitesides, R.; Frenklach, M. *J. Phys. Chem. A* **2010**, *114*, 689-703.

[39] Agafonov, G. L.; Naydenova, I.; Vlasov, P. A.; Warnatz, J. *Proc. Comb. Inst.* **2007**, *31*, 575-583. It is there stated, on the basis of a detailed kinetic modeling study, that "Soot precursors are formed in PAH molecule-radical and PAH radical-radical reactions".

[40] Frenklach, M. *Phys. Chem. Chem. Phys*. **2002**, *4*, 2028-2037. See in particular (a) sections 2.1 and 2.2; (b) section 3, p 2032, on particle nucleation.

[41] Xi, J.; Zhong, B.-J. *Chem. Eng. Technol.* **2006**, *29*, 665-673.

[42] Dobbins, R. A. *Aerosol Sci. Tech.* **2007**, *41*, 485-496.

[43] Wang, H. *Proc. Comb. Inst.* **2011**, *33*, 41–67.

[44] Bittner, J. D.; Howard, J. B. *Symp. Int. Combust. Inst.* **1981**, *18*, 1105-1116.

[45] Frenklach, M.; Wang, H. *Proc. Comb. Inst.* **1990**, *23*, 1559–1566.

[46] You, X.; Whitesides, R.; Zubarev, D.; Lester, W. A. jr; Frenklach, M. *Proc. Comb. Inst.* **2011**, *33*, 685–692.

[47] Howard, J. B. *23rd Symposium (Internat.) on Combustion / The Comb. Inst.* **1990**, 1107–1127. Pope, C. J.; Marr, J. A.; Howard, J. B. *J. Phys. Chem.* **1993**,*97,* 11001-11013. McKinnon, J. T.; Meyer, E.; Howard, J. B. *Comb. Flame* **1996**, *105*, 161-166.

[48] Siegmann, K.; Hepp, H.; Sattler, K. *Comb. Sci. Tech.* **1995**, *109*, 165-181. Hepp, H.; Siegmann, K.; Sattler, K. *Chem. Phys. Lett.* **1995**, *233*, 16-22.

[49] Violi, A.; D'Anna, A.; D'Alessio, A. *Chem. Eng. Sci.* **1999**, *54*, 3433-3442.

[50] D'Alessio, A.; D'Anna, A.; D'Orsi, A.; Minutolo, P.; Barbella, R.; Ciajolo, A. *Proc. 24th Int. Symp. Comb.* **1992**, 1973-1980. Pittsburgh, The Combustion Institute. For instance, regarding reactive coagulation, the Authors comment: "*A new conceptual model has been advanced for the formation of soot and high molecular mass structures in rich combustion to account for these experimental evidences. Polymeric structures with monomeric two- and three-ring functionalities are formed very early in the main oxidation zone, and soot inception is characterized by the progressive aromatization of these polymers. In other words, the formation of high molecular mass compounds occurs through the polymerization of small PAHs, more than the progressive growth of PAHs, as modeled with the HACA mechanism.*"

[51] D'Anna, A.; Violi, A.; D'Alessio, A. *Combust. Flame* **2000**, *121*, 418–429.

[52] D'Anna, A.; Violi, A.; D'Alessio, A.; Sarofim, A. F. *Combust. Flame* **2001**, *127*, 1995–2003.

[53] Violi, A. *Comb. Flame* **2004**, *139*, 279-287.

[54] Donnet, J. B. *Carbon* **1982**, *20*, 267-282.

[55] Indarto, A.; Giordana, A.; Ghigo, G.; Maranzana, A.; Tonachini, G. *Phys. Chem. Chem. Phys.* **2010**, *12*, 9429–9440.

[56] Giordana, A.; Maranzana, A.; Tonachini G. *J. Phys. Chem. C* **2011**, *115*, 1732–1739.

[57] Non-bonded interactions between molecules can either involve permanent dipoles or multipoles, or be exerted between a permanent dipole and an induced one, or originate from instantaneous, transient induction of dipoles (dispersive interaction). In specific cases, some or all of them can be present. Since all of them are often collected under the name of van der Waals interactions, we make extensive use of this more inclusive term throughout the paper.

[58] A PAH-like radical can be obtained from a closed shell even-C PAH by radical addition, or H-abstraction by a radical -both can be operated, for instance, by a H atom- or it can exist as such because of its structure. See for instance: Giordana, A.; Maranzana, A.; Ghigo, G.; Causà, M.; Tonachini, G. *J. Phys. Chem*. A **2008**, *112*, 973-982. As an example, 1-*H*-pyrenyl would closely resemble a vinyl-substituted phenalenyl radical.

[59] Pople, J. A.; Gill, P. M. W.; Johnson, B. G. *Chem. Phys. Lett.* **1992**, *199*, 557-560. Schlegel, H. B.; in *Computational Theoretical Organic Chemistry*, ed. I. G. Csizsmadia, R. Daudel, Reidel Publishing Co., Dordrecht, The Netherlands, 1981, pp. 129-159. Schlegel, H. B. *J. Chem. Phys.* **1982**, 77, 3676-3681. Schlegel, H. B.; Binkley, J. S.; Pople, J. A. *J. Chem. Phys.* **1984**, *80*, 1976-1981. Schlegel, H. B. *J. Comput. Chem*. **1982**, *3*, 214-218.

[60] Parr, R. G.; Yang, W. *Density Functional Theory of Atoms and Molecules*, Oxford University Press: New York, 1989, ch. 3.

[61] Zhao, Y.; Truhlar, D. G. *Theor. Chem. Acc.* **2008**, *120*, 215-41.

[62] A special issue of ***PCCP*** dedicated to the subject *Stacking Interactions* has appeared: Hobza, P. editor. *Phys. Chem. Chem. Phys.* **2008**, *10*, 2581-2865.

[63] Hohenstein, E. G.; Chill, S. T.; Sherrill, C. D. *J. Chem. Theory Comput.*, **2008**, *4*, 1996–2000. See also: http://comporgchem.com/blog/?cat=28&paged=3.

[64] Peverati, R.; Baldridge, K. K. *J. Chem. Theory Comput.* **2008**, *4*, 2030-2048.

[65] Gu, J.; Wang, J.; Leszczynski, J.; Xie, Y.; Schaefer, H.F. III *Chem. Phys. Lett.* **2008**, *459*, 164-166 and 2009, *473*, 209-210. Riley, K. E. ; Pitonák, M.; Cerný, J.; Hobza, P. *J. Chem. Theory Comput.* **2010**, *6*, 66–80.

[66] 3-21G sp basis set: Binkley, J. S.; Pople, J. A.; Hehre, W. J. *J. Am. Chem. Soc.,* **1980**, *102*, 939-947.

[67] Reaction enthalpies, entropies, and free energies were computed as outlined in: Foresman, J. B.; Frisch, Æ. *Exploring Chemistry with Electronic Structure Methods*; Gaussian, Inc.: Pittsburgh, PA, 1996; pp 166-168. See also: McQuarrie, D. A. *Statistical Thermodynamics*; Harper and Row: New York, 1973; Chapter 8.

[68] Boys, S. F.; Bernardi, F. *Mol. Phys.* **1970**, *19*, 553-566. Simon, S.; Duran, M.; Dannenberg, J. J. *J. Chem. Phys.* **1996**, *105*, 11024-11031. Kobko, N.; Dannenberg, J. J. *J. Phys. Chem. A* **2001**, *105*, 1944-195.

[69] Valdés, H.; Klusák, V.; Pitonák, M.; Exner, O.; Starý, I.; Hobza, P.; Rulíšek, L. *J. Comput. Chem.*, **2008**, *29*, 861-870.

[70] Gaussian 09, Revision A.02, Frisch, M. J.; Trucks, G. W.; Schlegel, H. B.; Scuseria, G. E.; Robb, M. A.; Cheeseman, J. R.; Scalmani, G.; Barone, V.; Mennucci, B.; Petersson, G. A.; Nakatsuji, H.; Caricato, M.; Li, X.; Hratchian, H. P.; Izmaylov, A. F.; Bloino, J.; Zheng, G.; Sonnenberg, J. L.; Hada, M.; Ehara, M.; Toyota, K.; Fukuda, R.; Hasegawa, J.; Ishida, M.; Nakajima, T.; Honda, Y.; Kitao, O.; Nakai, H.; Vreven, T.; Montgomery, J. A. jr.; Peralta, J. E.; Ogliaro, F.; Bearpark, M.; Heyd, J. J.; Brothers, E.; Kudin, K. N.; Staroverov, V. N.; Kobayashi, R.; Normand, J.; Raghavachari, K.; Rendell, A.; Burant, J. C.; Iyengar, S. S.; Tomasi, J.; Cossi, M.; Rega, N.; Millam, N. J.; Klene, M.; Knox, J. E.; Cross, J. B.; Bakken, V.; Adamo, C.; Jaramillo, J.; Gomperts, R.; Stratmann, R. E.; Yazyev, O.; Austin, A. J.; Cammi, R.; Pomelli, C.; Ochterski, J. W.; Martin, R. L.; Morokuma, K.; Zakrzewski, V. G.; Voth, G. A.; Salvador, P.; Dannenberg, J. J.; Dapprich, S.; Daniels, A. D.; Farkas, Ö.; Foresman, J. B.; Ortiz, J. V.; Cioslowski, J.; Fox, D. J. Gaussian, Inc., Wallingford CT, 2009.

[71] MOLDEN: Schaftenaar, G.; Noordik, J. H. *J. Comput.-Aided Mol. Design* **2000**, *14*, 123-134. (http://www.cmbi.ru.nl/molden/molden.html)

[72] Maranzana, A.; Serra, G.; Giordana, A.; Tonachini, G.; Barco, G.; Causà, M. *J. Phys. Chem. A* **2005**, *109*, 10929-10939.

[73] Pixner, P. ; Schiessl, R. ; Dreizler, A. ; Maas, U. *Comb. Sci. Tech.* **2000**, *158*, 485-509. Berlow, R. S.; Fiechtner, G. J.; Chen, J.-Y. *26th Symposium (Internat.) on Combustion / The Comb. Inst.* **1996**, 2199–2205. Choudhuri, A. R.; Gollahalli, S.R. *Int. J. Hydrogen En*. **2004**, *29*, 1293–1302. Zeegers, P. J. Th.; Alkemade C. Th. J. *Comb. Flame* **1965**, 9, 247-257. Seepana, S.; Jayanti S. *En. Conv. Manag.* **2009**, *50*, 1116–1123.

[74] Violi, A.; Truong, T. N.; Sarofim, A. *J. Phys. Chem. A* **2004**, 108, 4846-4852.

[75] Richter, H.; Granata, S.; Green, W. H.; Howard, J. B. *Proc. Combust. Inst.* **2005**, *30*, 1397–1405.

[76] D'Anna, A.; Kent, J. H. *Combust. Flame* **2008**, *152*, 573–587.

[77] Sirignano, M.; Kent, J.; D'Anna, A. *Comb. Flame* **2010**, *157*, 1211–1219.

[78] A reported peak value for ethyne concentration in a diffusion flame (Smooke, M. D.; McEnally, C. S.; Pfefferle, L. D.; Hall, R. J.; Colket, M. B. *Combust. Flame* **1999**, *117*, 117-139) is as high as 12,000 ppm. Molar fractions $\mathbf{x}_i$ for a number of species i were then assessed in recent years by Fei Qi and coworkers, working with different flames, as specified below.
Ethyne flame: Li, Y.; Zhang, L.; Tian, Z.; Yuan, T.; Zhang, K.; Yang, B.; Qi, F. *Proc. Comb. Inst.* **2009**, *32*, 1293–1300.
Benzene flame: Yang, B.; Li, Y.; Wei, L.; Huang, C.; Wang, J.; Tian, Z.; Yang, R.; Sheng, L.; Zhang, Y.; Qi, F. *Proc. Comb. Inst.* **2007**, *31*, 555–563.
Toluene flame: Li, Y.; Zhang, L.; Tian, Z.; Yuan, T.; Wang, J.; Yang, B.; Qi, F. *Energy & Fuels* **2009,** *23,* 1473–1485.
Gasoline flame: Li, Y.; Huang, C.; Wei, L.; Yang, B.; Wang, J.; Tian, Z.; Zhang, T.; Sheng, L.; Qi, F. *Energy & Fuels* **2007,** *21,* 1931-1941.
Molar fractions $\mathbf{x}_i$ for ethyne and ethene are reported here below.

***flame*:**	$C_2H_2/O_2/Ar$	$C_6H_6/O_2/Ar$	$C_6H_5\text{-}CH_3/O_2/Ar$	$gasoline/O_2/Ar$
ethyne	-	2.4×10^{-2}	3.8×10^{-2}	2.0×10^{-2}
ethene	1.2×10^{-3}	4.2×10^{-3}	1.5×10^{-3}	1.2×10^{-2}

[79] The model systems 1-5 are generally without an overall symmetry. Morever, if compared with simple alkanes, they present, in addition to steric, repulsive, interactions, the on-the-whole-attractive van der Waals interactions between the two PAH-like parts. These two factors cause some inadequacy of the usual syn, gauche, and anti terms. In fact, some structures can be classified by them with some difficulty, while other conformations could be legitimately expected, but are not found. For instance, in cases when we use the anti(periplanar) and syn(periplanar) terms appropriately, as e.g. for n-butane, we make reference to a plane, but if we use them for our systems in the loose way described in Chart 2, it cannot be identified with a plane of symmetry. Instead, what might be called a "plane zone" can be visualized in a fuzzy

way. The arrangement corresponding to the gauche label is even more vague. Moreover, if we find a gauche arrangement "on one side" of the plane zone, we can well be unable to find another on the other side, because it converges for instance on the syn upon optimization. The same for the "missing anti", in system 5, since it converges on sort of a gauche at all times.

[80] Sauers, R. R. *J. Chem. Educ.*, **1996**, *73*, 114-115.

[81] For instance, in ref. **76**, Fig. 2, temperature rises very steeply within the first mm of the "height above burner" **z** parameter, attaining the value of 1700 K around **z** = 1-2 mm. Then it goes down more slowly and to a limited extent, keeping not far from constant in the range **z** = 4-14 mm, depending on the conditions.

[82] Warnatz, J.; Maas, U.; Dibble R. W. *Combustion* 4th edition, Springer Verlag 2006 (see Ch. 7, pp 95, 96, and 108, 109).

[83] We should know if equilibrium is actually attained at some T, knowing that it can be attained for some species and not for others, as exemplified in Fig. 8.2, p 424, of ref. 12c. We have considered, in our models, the adduct formation as an isolated system, and we have set for simplicity $R \equiv P$ to consider actually a dimerization step:

$$2\ R \underset{k_r}{\overset{k_f}{\rightleftharpoons}} RR$$

Then, we have set the differential equation:

$$-\frac{d[R]}{dt} = k_f[R]^2 - k_r[RR] \qquad [R]_0 = [R] + 2[RR]$$

$$-\frac{d[R]}{dt} = k_f[R]^2 - \frac{1}{2}k_r([R]_0 - [R])$$

On this basis, we try to assess if equilibrium can be attained in a sufficiently short time, say t_{eq}, to be compared with the residence time, say t_r, of our system in some flame zone (which could be of the order of 10^{-5} s). This seems a reasonable assumption, based on what reported in ref. 82. We have collected the detailed results of such a simulation, based on some hypothesis about the initial concentration of R, R_0, in the Supporting Information. It comes out that the critical temperature, say T_c, above which the concentrations of the species involved depart from their equilibrium values by less than 1% within a time t_r is $T_c \approx 1000$ K. At that temperature, $t_{eq} < t_r$. In conclusion, an analysis based on pK's is more reliable beyond ~1000 K, and is likely to be inappropriate below this T. Yet, we have kept the plots in this paper (Fig. 6) still stretching down to 300 K, to emphasize that, for the lowest T values, the situation would be in principle (*if equilibrium were attained*) very favorable to adduct formation. On one hand, G is there dominated by the energetic factor (which is the only factor considered in some papers). But at those temperatures equilibrium is not attained. Then the situation is sharply modified at higher temperatures, where the $T\Delta S$ term manifests its weight. When T goes up to 1000 K and more, equilibrium is more easily attained, and the situation is, as commented, less favorable to adduct formation.

[84] Sabbah, H.; Biennier, L.; Klippenstein, S. J.; Sims, I. R.; Rowe B. R. *J. Phys. Chem. Lett.* **2010**, *1*, 2962–2967.

[85] Ishiguro, T.; Suzuki, N.; Fujitani, Y.; Morimoto, H. *Comb. Flame* **1991**, *85*, 1-6. See in particular mid p 4. Vander Wal, R. L. *Comb. Sci. Tech.* **1998**, *132*, 315-323. Popovitcheva, O. B.; Persiantseva, N.M.; Trukhin, M. E.; Rulev, G. B.; Shonija, N. K.; Buriko, Y. Y.; Starik, A. M.; Demirdjian, B.; Ferry, D.; Suzanne, J. *Phys. Chem. Chem. Phys.* **2000**, *2*, 4421-4426 (see in particular mid p 4423). Wentzel, M.; Gorzawski, H.; Naumann, K.-H.; Saathoff, H.; Weinbruch, S. *J. Aerosol Sci.* **2003**, *34*, 1347-1370. Ginzburg, B. M.; Tuĭchiev, Sh.; Tabarov, S. Kh.; Shepelevskii, A. A. *Chrystallography Reports* **2007**, *52*, 187-190.

[86] Naydenova, X.I.; Nullmeier, M.; Warnatz, J.; Vlasov, P.A. *Combust. Sci. Technol.* **2004**, *176*, 1667-1703. See in particular pp 1669-1670.

[87] Müller, J.-O.; Su, D. S.; Wild, U.; Schlögl, R. *Phys. Chem. Chem. Phys.* **2007**, *9*, 4018–4025.

[88] Cain, J. P.; Gassman, P. L.; Wang, H.; Laskin, A. *Phys. Chem. Chem. Phys.* **2010**, *12*, 5206–5218 (in particular, fig. 9).

[89] Vander Wal, R. L.; Tomasek, A. J. *Comb. Flame* **2004**, *136*, 129-140.

[90] Ishiguro, T.; Takatori, Y.; Akihama, K. *Comb. Flame*. **1997**, *108*, 231-234.

[91] Gao, G. T.; Mikulski, P. T.; Chateauneuf, G. M. ; Harrison, J. A. *J. Phys. Chem. B* **2003,** *107,* 11082-11090.

[92] di Stasio, S. *J. Aerosol Sci*. **2001**, *32*, 509-524.

[93] Dalis, A.; Friedlander, S. *J. Aerosol Sci*. **2005**, *36*, 27-42.

[94] di Stasio, S.; Iazzetta, A. in: *Chemical Engineering Transactions 10*, AIDIC: Milano, 2006, pp. 483-488. ISBN 88-901915-7-0.

[95] Griffiths, J. F.; Barnard, J. A. *Flame and Combustion*, 3rd edition, Blackie Academic & Professional, Chapman & Hall, 1995, Ch 6.

[96] Kendall, R. A.; Dunning, T. H., Jr.; Harrison, R. J. *J. Chem. Phys.* **1992**, *96*, 6796-806.

[97] Woon, D. E.; Dunning, T. H., Jr. *J. Chem. Phys.* **1993**, *98*, 1358-1371.

[98] Halkier, A.; Helgaker, T.; Jørgensen, P.; Klopper, W.; Koch, H.; Olsen, J.; Wilson, A. K. *Chem. Phys. Lett.* **1998**, *286*, 243-252.